Spatiotemporal Metabolic Responses to Water Deficit Stress in Distinct Leaf Cell-types of Poplar

Vimal Kumar Balasubramanian[1†], Dusan Velickovic[1†], Maria Del Mar Rubio Wilhelmi[2], Christopher R Anderton[1], C. Neal Stewart, Jr.[3,4], Stephen DiFazio[5], Eduardo Blumwald[2] and Amir H. Ahkami[1,6*]

Key Words: Palisade mesophyll, Vascular, MALDI-MSI imaging, Spatial Metabolomics, Secondary metabolites, Drought

[1] Environmental Molecular Sciences Laboratory (EMSL), Pacific Northwest National Laboratory (PNNL), Richland, Washington, USA.

[2]Department of Plant Sciences, University of California, Davis, California, USA.

[3] Department of Plant Sciences, University of Tennessee, Knoxville, Tennessee, USA.

[4] Center for Agricultural Synthetic Biology, University of Tennessee, Knoxville, Tennessee, USA.

[5]Department of Biology, West Virginia University, Morgantown, West Virginia, USA.

[6]Adjoint Faculty, School of Biological Science (SBS), Washington State University (WSU), Pullman, Washington, USA.

† These authors contributed equally to the manuscript.

*Corresponding author: Amir H. Ahkami (amir.ahkami@pnnl.gov)

Abstract

The impact of water-deficit (WD) stress on plant metabolism has been predominantly studied at the whole tissue level. However, plant tissues are made of several distinct cell types with unique and differentiated functions, which limits whole tissue 'omics'-based studies to determine only an averaged molecular signature arising from multiple cell types. Advancements in spatial omics technologies provide an opportunity to understand the molecular mechanisms underlying plant responses to WD stress at distinct cell-type levels. Here, we studied the spatiotemporal metabolic responses of two poplar leaf cell types -palisade and vascular cells- to WD stress using matrix-assisted laser desorption Ionization-mass spectrometry imaging (MALDI-MSI). We identified unique WD stress-mediated metabolic shifts in each leaf cell type when exposed to early and prolonged WD and recovery from stress. During stress, flavonoids and phenolic metabolites were exclusively accumulated in leaf palisade cells. However, vascular cells mainly accumulated sugars during stress and fatty acids during recovery conditions, highlighting a possibility of interconversion between sugars and fatty acids under stress and recovery conditions in vascular cells. By comparing our MALDI-MSI metabolic data with whole leaf tissue gas chromatography-mass spectrometry (GC-MS)-based metabolic profile, we identified only a few metabolites that showed a similar accumulation trend at both cell-type and whole leaf tissue levels. Overall, this work highlights the potential of the MSI approach to complement the whole tissue-based metabolomics techniques and provides a novel spatiotemporal understanding of plant metabolic responses to WD stress. This will help engineer specific metabolic pathways at a cellular level in strategic perennial trees like poplars to help withstand future aberrations in environmental conditions and to increase bioenergy sustainability.

Introduction

Water-deficit (WD) stress is detrimental to plant growth and productivity. Plant responses to WD are dynamic and involve complex cross-talk between different regulatory pathways (Long, 2011), including metabolic adjustments and gene/protein expression at the molecular level for physiological and morphological adaptation at the whole-plant level (Dinneny et al., 2008). However, each cell-type in plant tissues is defined by specific transcriptional, protein, and metabolic profiles that determine its function and response(s) to stress (Plant Cell Atlas et al., 2021). With the establishment of the Plant Cell Atlas (PCA) community (Rhee et al., 2019), the importance of location-to-function paradigm has been highlighted, suggesting that this model has the potential to unlock new discoveries in plant sciences including how plants respond to environmental perturbations like WD (Plant Cell Atlas et al., 2021). Indeed, recent plant single-cell studies, which have been mostly performed in model species, indicate that plant responses to internal and external cues are largely cell type-specific (Xu and Jackson, 2023, Yang et al., 2021, Farmer et al., 2021, Nolan et al., 2023). Thus, determining the plant responses to WD requires the study of the cell/molecular properties of specific cell-types within a tissue to effectively reveal the underlying mechanisms regulating physiological processes and plasticity under suboptimal conditions.

Poplar (*Populus spp*.), a prevalent woody feedstock for improved next-generation biofuels, is one of the most biomass-productive native tree taxa in the northern hemisphere. While poplar species are good targets for carbon sequestration (Wullschleger et al., 2005) and production of feedstocks for biofuels and biomaterials (Bryant et al., 2020), they have also been widely used in physiological studies to understand how perennial trees respond to environmental changes (Li et al., 2014). Whole tissue responses to WD stress have been investigated in *Populus* at epigenome (Sow et al., 2021), transcriptome (Robertson et al., 2022, Rosso et al., 2023, Lee et al., 2021, Yang et al., 2023, Jia et al., 2017, Cossu et al., 2014, Wilkins et al., 2009), proteome (Plomion et al., 2006, Gao et al., 2022, Li et al., 2014, Xiao et al., 2009, Durand et al., 2011), and metabolome (Jia et al., 2020, Barchet et al., 2013, Hamanishi et al., 2015,

He et al., 2022, Law, 2020, Tschaplinski et al., 2019b, Barchet et al., 2014) levels. However, spatiotemporal molecular mechanisms controlling plant responses to WD stress is not yet thoroughly understood in *Populus* and similar perennial trees.

Metabolites represent the downstream products of multiple interactions between genes, transcripts, and proteins. Small changes in gene and protein expression at functional levels are basically amplified at the metabolite level, which nominates metabolites as the ideal predictive molecular markers for stress response phenotypes compared to transcripts or proteins alone. Moreover, nonfunctional changes in many genes and proteins are not reflected in metabolites (Shen et al., 2023). Therefore, metabolomics has been considered as a very powerful approach for identifying the key primary and secondary small bioactive molecules with important roles in plant responses to environmental changes (Ahkami et al., 2019, Kumar et al., 2021, Barchet et al., 2013). The effect of WD stress at the metabolite level has been studied extensively in whole tissues using conventional extraction and metabolomics assays that include gas and liquid chromatography-based mass spectrometry (GC- and LC-MS) techniques (Jia et al., 2020, Hamanishi et al., 2015, Barchet et al., 2013, Nakayasu et al., 2016). Several studies in poplar reported whole leaf tissue level metabolomic shifts in response to WD stress conditions (He et al., 2022, Law, 2020, Tschaplinski et al., 2019b, Barchet et al., 2014). For instance, metabolomic analysis of whole leaf tissue of the WD-tolerant (*Populus simonii*) and -susceptible (*Populus deltoides* cv. 'Danhong') varieties suggested potential roles of increased antioxidants and long chain fatty acids in response to WD (Jia et al., 2020). Moreover, metabolomic analysis identified an increased level of raffinose family oligosaccharides in leaves of *P. balsamifera* under WD (Hamanishi et al., 2015). In another study with hybrid poplar (*P. deltoides* var. occidentalis and *P. × petrowskyana*), phenolic compounds, raffinose family-related compounds, and certain antioxidant metabolites were found to be involved in plant responses to WD stress (Barchet et al., 2013). However, our understanding of cell type specific metabolic changes under WD is scarce. Essentially, leaf cell types vary widely in their biological functions, in which

97 palisade mesophyll cells are involved mainly in photosynthesis, while vascular cells are involved in inter-
98 tissue signaling via xylem and phloem sap exchange. Therefore, cell-specific responses to WD at metabolic
99 level may be critical for understanding their roles in plant stress tolerance.

100 Matrix-assisted laser desorption/ionization (MALDI) mass spectrometry imaging (MSI) is a robust
101 molecular imaging technology that uses a focused laser beam to ablate and ionize material into the mass
102 analyzer, which can provide high spatial resolution of the location of endogenous molecules from tissues
103 *in situ*. Combined with spatial probing, a MALDI-MSI experiment enables simultaneous visualization of
104 hundreds of molecules mapped to tissue morphology (Veličković et al., 2021). This approach has been
105 used to evaluate the surface distribution of polysaccharides (Veličković et al., 2014), small sugars and
106 glucosides (Bøgeskov Schmidt et al., 2018), metabolites, and lipids (Veličković et al., 2021) in different
107 plant tissues and organs. For example, MALDI-MSI was used in barley roots to uncover the spatial
108 distribution of metabolites in response to salinity stress (Sarabia et al., 2018). A recent advancement in
109 spatial metabolic imaging approach using MALDI-MSI has been used to identify WD stress responses in
110 *Piper sp.* and *Hibiscus rosa* sinensis root tissue (Honeker et al., 2022). The results showed a vascular and
111 epidermis cell-specific accumulation of lignin-like metabolites, antioxidants, and fatty acid metabolites in
112 each plant species, thereby highlighting the potential use of such a spatial imaging platform to visually
113 map the metabolites in different cell types of WD-exposed plant tissues.

114 Here, we report spatiotemporal changes in metabolites levels in poplar leaf tissue when exposed
115 to WD and recovery from stress. We describe the palisade specific accumulation of flavonoid and other
116 phenolic compounds during WD treatment. In addition, accumulation of sugars together with the
117 decreased number of fatty acids may indicate synthesis and transport of sugar via gluconeogenesis
118 pathway during WD. Vascular cells showed an interconversion between fatty acids and sugar levels during
119 WD and recovery period. Overall, our results unravel cell-specific spatiotemporal metabolic changes in
120 response to WD. Further, we report the use of MALDI-MSI as a powerful technique when combined with

121 conventional GC-MS-based whole tissue metabolic profiling to gain a granular understanding of plant
122 responses to WD stress. This work highlights the power of a spatial metabolomics approach in
123 understanding plant responses to abiotic stresses, enabling future attempts at mapping molecular
124 machineries to cellular domains. These mechanistic molecular insights can be exploited to aid the design
125 of strategic bioenergy trees with enhanced tolerance to WD stress.
126
127 **Materials and methods**
128 ***Plant growth conditions and water-deficit stress treatment.***
129 Clones of *Populus tremula* x *alba* (INRA 717 1-B4) were rooted in sterile conditions in a growth
130 chamber (16-hr/8-hr day/night and 24°C/18°C 600 µmol $m^{-2}s^{-1}$) for at least 25 days. Seedlings were
131 transplanted into 1.5 L pots filled with Profile Porous Ceramic (PPC) soil. The seedlings were grown (16-
132 hr/8-hr day/night and 24°C/18°C 800 µmol $m^{-2}s^{-1}$) in the greenhouse and fertilized every day with a
133 nutrient solution containing N 77 ppm, P 20 ppm, K 75 ppm, Ca 27 ppm, Mg 17 ppm, S 65 ppm, Fe 1.50
134 ppm, Mn 0.50 ppm, Zn 0.05 ppm, Mo 0.01 ppm, Cu 0.02 ppm and pH 5.6. Water deficit treatments were
135 applied 45 days after rooting by withholding water until visual stress symptoms (i.e., leaf wilting) appeared
136 (30–35% relative soil water content) (early water deficit, E-WD). Plants were kept for ten days at 35% soil
137 water content (late water deficit, L-WD) and then re-watered with regular fertilization for three days after
138 sampling for the recovery period (REC). Samples from each treatment were collected between 9-10 am (1
139 and ½ –2 and ½ hours after the light turned on). Midrib-containing leaf punches were harvested, flash
140 frozen in liquid nitrogen, and kept at −80°C until use. These leaf punches (disks with ~0.5-inch diameter in
141 size) were used for MALDI-MSI workflow for spatial metabolomic analysis. Alternatively, whole
142 intermediate leaves from an independent WD experiment were harvested, immediately frozen in liquid
143 nitrogen, and kept at −80°C until use. These whole leaf tissues were used for GC-MS-based metabolomic
144 profiling. At any given stress or recovery timepoints, leaf punches were collected from six biological

145 replicates for MALDI-MSI, while the entire leaf from three independent biological replicates were
146 collected for whole leaf metabolite profiling. Leaf gas exchange parameters were collected from four
147 biological replicates.
148
149 ***Gas-exchange and biomass measurements.***
150 Photosynthesis measurements were recorded in intact plants using a portable gas exchange
151 system (LI-COR 6400). Photosynthesis was induced by saturating light (1000 µmol m^{-2} s^{-1}) with 400 µmol
152 mol^{-1} CO_2 surrounding the leaf (Ca). The amount of blue light was set to 10% photosynthetically active
153 photon flux density to optimize stomatal aperture. Block temperature was set to 24 °C. Plant samples for
154 biomass assay were collected and oven dry at 60 °C for 5 days.
155
156 ***Cryosectioning of frozen leaf tissue and sample preparation for MALDI-MSI imaging.***
157 Leaves were embedded within a mixture of 7.5% hydroxypropyl methylcellulose (HPMC) and 2.5%
158 polyvinylpyrrolidone (PVP), and 12 µm sections were thaw mounted on indium tin oxide (ITO)-coated glass
159 slides using a cryotome maintained at -14°C (CryoStar NX-70 Cryostat, Thermo Scientific, Runcorn, UK).
160 Slides were vacuum dried and homogenously sprayed, using a M5 Sprayer (HTX Technologies, Chapel Hill,
161 NC), with 2,5-dihydroxybenzoic acid (DHB) matrix for analysis in positive ion mode(Veličković et al., 2021)
162 and N-(1-naphthyl) ethylenediamine dihydrochloride (NEDC) matrix for analysis in negative ion
163 mode(Honeker et al., 2022). DHB was prepared at a concentration of 40 mg/mL DHB (in 70% MeOH) and
164 was sprayed at 50 µL/min flow rate. The nozzle temperature was set to 70 °C, with 12 cycles at 3 mm track
165 spacing with a crisscross pattern. A 2 s drying period was added between cycles, a linear flow was set to
166 1,200 mm/min with 10 PSI of nitrogen gas and a 40 mm nozzle height. This resulted in matrix coverage of
167 ~667 µg/cm^2 for DHB. NEDC was prepared at a concentration of 7 mg/mL NEDC in 70% MeOH and was
168 sprayed at 120 µL/min flow rate. The nozzle temperature was set to 70 °C, with 8 cycles at 3 mm track

spacing with a crisscross pattern. A 0 s drying period was added between cycles, a linear flow was set to 1200 mm/min with 10 PSI of nitrogen gas and a 40 mm nozzle height. This resulted in matrix coverage of ~187 µg/cm^2 for NEDC.

MALDI-MSI data collection and processing.

All imaging analyses were performed on an ESI/MALDI dual-source MALDI Fourier transform ion cyclotron resonance (FTICR)-MS equipped with the ParaCell (scimaX 2XR 7T, Bruker Daltonics, Bremen, Germany) operating in MALDI mode with the data point sizes of 2 M and 2w detection. Positive ion mode acquisitions with DHB were acquired with broadband excitation from *m/z* 92 to 1,000, resulting in a detected transient of 0.418 s— the observed mass resolution was ~200k at *m/z* 400. Negative ion mode NEDC analyses were acquired with broadband excitation from *m/z* 92 to 1,000, resulting in a detected transient of 0.418 s— the observed mass resolution was ~200k at *m/z* 400. FlexImaging (Bruker Daltonics, v.5.0) was used for the imaging acquisition, and analyses were performed with 30 µm step size. FlexImaging sequences were directly imported into SCiLS Lab (Bruker Daltonics, v.2023.a Premium 3D) using automatic MRMS settings. Ion images were directly processed from the profile datasets within SCiLS Lab, and automated annotation of the centroided dataset was completed within METASPACE. KEGG-v1 and SwissLipids were used as databases for annotaions within 3 ppm m/z tolerance. List of annotated m/z features was imported back to the SCiLS, and table with ion intensity of each annotated feature (after RMS normalization) in palisade and vascular part of each leaf section was created and used further for statistical (t-test) analysis. Palisade and vascular region of the leaf were manually outlined in the SCiLS software (Bruker Daltonics) using brightfield microscopy image recorded for each analyzed section. Due to instrument and resource limitations, we were not able to collect leaf punches from the entire leaf for sectioning and MALDI-MSI. However, we used 6 biological replicates with 2 technical replicates (each consecutive sections, n=12) for any given condition. The relative abundance level of a metabolite in

193 palisade or vascular cell was calculated by summing the relevant abundance levels from a region of tissue
194 comprising cell-types of each kind (Supplementary Figure S2).
195
196 ***Whole leaf tissue metabolites profiling by GC-MS.***
197 Ground frozen powder of the intermediates leaves from poplar plants grown under control, and
198 water deficit (E-WD and L-WD) and recovery conditions were submitted to the West Coast Metabolomics
199 Center (University of California, Davis), extracted, measured, and analyzed by gas chromatography–mass
200 spectrometry (MS) (Gerstel CIS4–with a dual MPS Injector/Agilent 6,890 GC-Pegasus III TOF MS) as
201 described before (Weckwerth, Wenzel, & Fiehn, 2004). Processes for the integrated extraction,
202 identification, and quantification of metabolites were performed according to Fiehn et al. (2008).
203 Metabolites are expressed as differential abundancy of normalized intensity values (log2) between
204 Control and E-WD, L-WD and recovery treatments.
205
206 ***Van-Krevelen classification and pathway analysis.***
207 Van-Krevelen analysis was performed as reported (Honeker et al., 2022). Briefly the molecular
208 formula from significantly upregulated and downregulated metabolites (t-test, $p<0.05$) was used to
209 classify them into higher order metabolic classes such as lignins, hydrocarbons, tannins, carbohydrates,
210 proteins, etc., based on the elemental ratios O/C and H/C ratios. Molecular formulas that come under
211 broader classes, such as lignins, were looked up in KEGG pathways to identify specific sub-class, such as
212 flavonoids, to derive pathway maps in Figures 2 and 3.
213
214 ***Statistical analysis.***
215 For biomass, leaf gas exchange parameters, and MALDI-MSI relative metabolite abundance
216 analysis, the significance test was performed using T-tests with the built-in statistical function in Microsoft

Excel. For the whole leaf tissue metabolomics analysis (GC-MS), the significance test was performed using one-way ANOVA analysis. ANOVAs of individual features were performed using aov function of STATS package in R (R Core Team 2021). In this manuscript, we present significantly changed data under stress or recovery conditions ($P < 0.05$) compared with controls; however, in the case of MALDI-MSI analysis, we also include the moderately changed data ($0.5 < P \leq 0.1$) compared with controls.

Results

Plant biomass and photosynthesis rates were affected by water deficit stress.

Whole plant responses to water limitation were monitored via biomass and gas exchange parameter measurements during early WD (E-WD), late WD (L-WD), and recovery (R) conditions. Compared to the control well-watered condition, plant shoot biomass was reduced under E-WD (-48%), L-WD (-67%) and R (-75%) treatments (Figure S1A, B; Supplementary table S1). Root biomass was reduced during E-WD (-44%) and R (-65%) but showed no change during L-WD compared to control roots (Fig S1B). Among physiological parameters, leaf tissue showed a decrease in net photosynthesis (A_N) (-75%, -23%), stomatal conductance (g_s) (-95%, -61%), and leaf transpiration (-91%, -51%) during E-WD and L-WD stages, respectively. In contrast, during recovery from stress, higher values of g_s (+80%) and leaf transpiration (+58%) were observed compared to non-stressed control plants (Supplementary Figure S1B and Supplementary table S1).

A spatiotemporal metabolic shift was detected in poplar leaf cell types.

Leaf tissues were harvested from plants under WD and recovery conditions, cryosectioned, and used for MALDI-MS imaging-based spatial metabolomics. We looked for metabolites that were significantly altered by WD treatment compared to controls, especially in palisade mesophyll and vascular regions of cryosectioned leaf tissue (Supplementary Figure S2). By combining positive and negative

ionization mode analyses in MALDI, a total of 2,358 spectral features were detected, which were then curated to remove false positives and spotty non-real abundance patterns. This left 103 molecular features that were significantly altered in palisade and/or vascular cell types under E-WD/L-WD and/or recovery time points compared to the control well-watered (WW) condition (Supplementary Table S2). Of those, 60 molecular features were significantly altered in a cell type-specific manner (strictly enriched or depleted in palisade or vascular cell type), while 43 metabolites were significantly altered in both leaf cell types. Between time points, recovery condition had more metabolites altered in both palisade (n=29) and vascular (n=57) cell types compared to E-WD and L-WD conditions (Figure 1A). However, between the two cell types, vascular cells showed a higher number of significantly altered metabolites than palisade cells under any harvesting timepoints (Figure 1A). We categorized the identified molecular features into metabolic classes through Van Krevelen classification (Honeker et al., 2022), which groups molecular formulas based on their elemental ratios (O/C and H/C ratios) and degree of unsaturation. The categories included different biochemical classes such as secondary metabolites (lignin, condensed hydrocarbons, unsaturated hydrocarbons), lipids, and carbohydrate-related metabolites (Figure 1B, Supplementary Table S2). This analysis showed a higher number of WD- or recovery-altered metabolites belonged to lignins (n=39) and condensed hydrocarbons (n=33), followed by carbohydrates (n=16), lipids (n=3), and other metabolic classes (n=8) (Figure 1B). The MALDI-MSI technique used in this study cannot resolve between stereoisomers, which means that the relative abundance levels of a molecular feature represent an average abundance of all stereoisomers (e.g., $C_6H_{12}O_6$ isomers include monosaccharides such as glucose, fructose, mannose, etc.). Therefore, any significant changes in the cellular abundance level of $C_6H_{12}O_6$ represent a significant shift in total monosaccharide levels in a particular cell type. Based on the metabolite classification outcome (Figure 1B) and to further identify distinct spatial trends in leaf cell types, we mainly focused on secondary metabolites, lipids, and carbohydrate-related metabolites in two major leaf cell types, i.e., palisade mesophyll and vascular cell types, when exposed to WD conditions. We

identified a palisade cell type specific metabolic trend in flavonoid biosynthesis pathway, while in vascular cells, lipid and sugar metabolism altered in a cell type specific manner.

Water deficit stress elevated the levels of specific flavonoids and fatty acids uniquely in leaf palisade cells.

Many plant species, including poplars, were shown to elevate the levels of different flavonoids in whole leaf tissues under water-limited conditions that help scavenge the ROS generated during stress(Ahmed et al., 2021b, Shomali et al., 2022, Tattini et al., 2004). Here, our spatial metabolomics approach allowed us to look for any cell type level differences in flavonoid distribution during WD stress and recovery time points in hybrid poplar leaf. Palisade mesophyll cells uniquely exhibited a higher relative abundance of specific flavonoids during E-WD, L-WD, and recovery stages (Figure 2A and Supplementary Table S2). Compared to the E-WD stage, prolonged WD stress induced the accumulation of a greater number of flavonoids in a cell-type specific manner. Among those, tremulacin was increased (+2.89-fold) in palisade cells during E-WD, while stereoisomers quercetin and tricetin, represented by the molecular formula $C_{15}H_{10}O_7$, were elevated (+1.45-fold) exclusively during L-WD stage. Prolonged WD also induced the abundance levels of $C_9H_8O_4$ that represent caffeate (+2.4-fold), and polyketides such as pseudopurpurin (+1.33-fold) exclusively in palisade cells (Figures 2A, 2B and Supplementary Table S2). During recovery from WD stress, a higher level of $C_{15}H_{10}O_6$, which represents stereo-isomeric flavonoids such as kaempferol and luteolin (+1.24-fold), $C_{14}H_8O_5$ which include purpurin (+1.28-fold), and two aromatic phytochemicals riccionidin A (+1.33-fold) and rhein (+1.37-fold) were exclusively detected in palisade cells (Figures 2A, 2B and Supplementary Table S2). Vascular cells did not show any significant changes in abundance levels of the abovementioned flavonoids during the WD or R stages (Figures 2A, 2B and Supplementary Table S2). Therefore, palisade cell-specific accumulation of these secondary metabolites, mostly during L-WD and recovery stages, highlights a spatially distinct metabolic activity in

palisade cells in response to WD stress and recovery in poplar. However, a number of other secondary metabolites that accumulated in vascular cells had reduced abundance in palisade cells. They include $C_{13}H_{18}O_7$, $C_7H_{14}N_2O_7$, and $C_7H_{11}NO_7P_2$, representing salicin (+1.62-fold), coumeroic acid (+2.24-fold), and risedronic acid (+1.71-fold), respectively (Supplementary Table S2).

Unsaturated fatty acids also play a role in stress response by scavenging ROS (He and Ding, 2020b). During L-WD stress, we noticed a moderate increase in $C_{18}H_{32}O_2$ representing the fatty acid linoleate (+1.22-fold) only in palisade cells (Figure 2A), while its abundance level did not change in vascular cells, highlighting a potential role for higher linoleate levels in palisade cells during L-WD stress. Moreover, two other fatty acids, hexadecanoic acid (-0.75-fold) and (6Z,9Z,12Z)-octadecatrienoic acid (-0.78-fold), showed reduced levels in palisade cells during the E-WD and R timepoints (Figure 2A, Supplementary Table S2). Altogether, the WD-stressed palisade cells showed a cell-type specific accumulation of flavonoids and the fatty acid linoleate, especially under L-WD and recovery stages, which was not observed in the vascular cell-type (Figures 2A, 2B and Supplementary table S1).

Vascular cells showed an opposite trend with the accumulation of fatty acids and sugars in response to water deficit stress.

Vascular cells transport a wide array of primary and secondary metabolites via xylem and phloem sap and provide structural support to the plant through secondary cell wall formation. Here, using a spatial metabolomics approach, we found an opposite trend with the levels of fatty acids and glycolytic metabolites in vascular cells especially during E-WD and Recovery conditions (Figure 3A, 3B). During E-WD stage, vascular cells showed reduced levels of three fatty acids, linoleate (-0.73-fold), hexadecanoic acid or palmitic acid (-0.84-fold), and $C_{18}H_{30}O_2$ that potentially represent (6Z,9Z,12Z)-Octadecatrienoic acid (-0.73-fold), a polyunsaturated fatty acid (Figure 3A, 3B & Supplementary Table S2). However, focusing on the glycolysis/gluconeogenesis pathways, we observed an increase in sugars and sugar-phosphate levels

under E-WD condition (Figure 3A,3B). The level of $C_{12}H_{22}O_{11,}$ which comprises disaccharide sugars such as sucrose and maltose showed a +1.34-fold increase, while $C_6H_{12}O_{6,}$ which comprise monosaccharide sugars such as glucose, fructose, and mannose, showed a +2-fold increase exclusively in vascular cells during E-WD condition (Figure 3A, 3B). Although these di- and mono-saccharides were also detected in palisade cells (Figure 2A), their abundance levels were not significantly altered under E-WD stress vs. control conditions. Moreover, sedoheptulose 7-phosphate and related isomers ($C_7H_{15}O_{10}P$) was also highly abundant in vascular cells (+1.56-fold) under E-WD stress condition. Under recovery condition, however, we found an opposite trend with the abundance levels of the abovementioned sugars and fatty acids, in a way that the levels of disaccharides (-0.63 fold) and monosaccharides (-0.69 fold) were reduced, while the relative abundance levels of all three fatty acid levels including linoleate (+1.48 fold), hexadecanoic acid (+1.18-fold), and (6Z,9Z,12Z)-octadecatrienoic acid (+1.74 fold) were increased. The observed opposite trend between fatty acid, mono, and disaccharide sugars, and sugar-phosphate levels during stress and recovery conditions indicate that vascular cells possibly break down the fatty acids to generate sugars via the gluconeogenesis pathway to support respiration during WD stress conditions. Moreover, the abundance level of $C_6H_8O_{7,}$ which represents the TCA cycle intermediate citrate and its isomers, was increased during recovery (+1.58 fold), highlighting a possible role of citrate in respiration and activation of fatty acid biosynthesis when plants are recovered from WD (Pracharoenwattana et al., 2005). The other TCA cycle-related metabolites, such as cis-aconitate and oxoglutarate, showed no significant changes in their abundance levels in stress and recovery stages (supplementary table S2).

Apart from fatty acids and sugar metabolites, vascular cells showed a reduced level of 27 different secondary metabolites during recovery from WD stress (Figure 3A and Supplementary Table S2). These include $C_{15}H_{12}O_{5,}$ which represents flavonoid naringenin chalcone (-0.58-fold), and several other phenylpropanoid pathway-derived metabolites such as dihydrokaempferol (-0.56-fold), 4',6-Dihydroxyflavone (-0.52-fold), and 4'-O-Methylisoflavone (-0.50-fold). (Supplementary table S2). Such an

overall reduction in secondary metabolite biosynthesis in vascular cells during recovery from stress indicates a possible spatiotemporal diversion of carbon flow to other essential primary metabolism pathways to support recovery from stress.

MALDI-mass spectrometry imaging as a complementary technique to traditional whole tissue metabolite profiling.

Whole tissue metabolomics approaches using GC-MS and LC-MS techniques have been widely used to address different questions in plant biology including plant responses to stress (Jorge et al., 2016, Ma and Qi, 2021). However, the outcomes of these studies have not been correlated with spatial and temporal distribution of metabolites in plant cell-types. Here, we performed a whole leaf tissue GC-MS-based metabolite profiling during E-WD, L-WD and recovery stages, and then compared the outcomes with our MALDI-MSI data. We hypothesized that spatial metabolomics verifies the whole tissue metabolic trends under WD condition and more importantly provides additional and key complementary information that are missed with traditional whole tissue-based approach. Out of 427 GC-MS-based metabolic features that changed significantly during stress and recovery conditions, 147 metabolites were identifiable through a library search. Among them, E-WD, L-WD, and recovery treatments resulted in 93, 74, and 55 significant metabolites, respectively (Supplementary Table S3, Supplementary Figure S3). We found 26 metabolites that were commonly detected by both GC-MS and MALDI approaches. However, compared to our spatial MALDI-MSI data, only seven metabolites showed a similar trend (increase or decrease) in their relative abundance levels in whole leaf tissue. They include glucose and mannose (increased during E-WD in whole leaf tissue) which regarding MALDI-MSI refer to monosaccharides ($C_6H_{12}O_6$) (increased in vascular cells during E-WD) (Figure 4A, 4B); palmitate or hexadecanoic acid (increased under recovery condition in whole leaf tissue) which regarding MALDI-MSI refers to $C_{16}H_{32}O_2$, (increased in vascular cells during recovery condition); and inositol-4-monophosphate, glucose-6-

phosphate, galactose-6-phosphate, and fructose-6-phosphate (reduced during L-WD in whole leaf tissue) which regarding MALDI-MSI collectively refer to sugar phosphates ($C_6H_{13}O_9P$) (reduced in both palisade and vascular cells during L-WD) (Figure 4A, 4B). This highlights the use of the MALDI-MSI as a powerful complementary tool to understand the spatial distribution of metabolites in plant tissues during environmental stresses.

Discussion

Recently, several studies highlighted the importance of understanding plant cell type-specific abiotic stress responses to maximize plant performance under suboptimal environmental conditions (Jeong et al., 2013, Fàbregas et al., 2018, Lee et al., 2016). In this work, we studied the metabolic responses of poplar to WD in a spatiotemporal manner and identified several distinct metabolites or pathways uniquely activated in leaf tissue cell types.

Leaf development and patterning involve co-ordination between meristematic cell division, cell expansion, and differentiation processes that form specialized cell-types. The adaxial side of the leaf tissue is packed with chloroplast-dense palisade mesophyll cells which are involved in photosynthesis. In contrast, the vascular cells mobilize the fixed photosynthate and other macro molecules to other tissues. Several recent single-cell transcriptomic studies performed in leaf tissue of model plants highlighted the distinct molecular profiles associated with different leaf cell types (Tenorio Berrío et al., 2021, Zang et al., 2023, Zhu et al., 2023), re-emphasizing that palisade and vascular cells are developmentally and functionally distinct, possibly exhibiting cell-type unique responses to environmental stresses such as WD.

During abiotic stresses such as WD, cellular ROS levels increase, which leads to oxidative damage of many cellular processes, including fatty acid peroxidation (Cruz de Carvalho, 2008). Previous metabolomic analysis at the whole tissue level suggested important roles for flavonoids and aromatic compounds in drought stress tolerance in several plant species (Ahmed et al., 2021a, Shomali et al., 2022,

Tattini et al., 2004). Using spatial metabolomics, we found an exclusive increase in the abundance of several secondary metabolites including flavonoids, polyketides, and phenylpropanoid pathway-related metabolites during L-WD stage in palisade cells (Figure 2A, 2B, Supplementary table S2). Among them, quercetin and luteolin are known to regulate ROS levels in plants by playing antioxidant roles (Singh et al., 2021, Hodaei et al., 2018, Gori et al., 2021). Other such as Riccionidin was found to confer abiotic stress tolerance in liverwort (*Marchantia polymorpha*), while anthraquinone derivatives such as purpurin and pseudopurpurin have been found to have antioxidant properties (Albert et al., 2018, Jin et al., 2011). The increased induction of secondary metabolism under prolonged drought in *Populus* was associated with adaptive mechanisms rather than metabolic perturbations, leading to increased organic solute accumulation (reduced osmotic potential) for improved drought tolerance (Tschaplinski et al., 2019a). Moreover, our results showed the accumulation of other aromatic compounds that remained undetected in previous studies where whole tissue metabolomics-based approaches were applied. For example, we found an increased level of tremulacin, a salicylate derivative (Feistel et al., 2015, Rubert-Nason et al., 2014), in a palisade-specific manner under E-WD condition. This highlights the role of palisade cells in exclusively directing carbon partitioning to secondary metabolism involved in ROS-neutralization and antioxidant responses to WD stress. Focusing on fatty acids, the levels of linoleate were increased in the palisade cells during the L-WD treatment, while no significant changes were observed in vascular cells (Supplementary Table S2). By anatomy, palisade mesophyll cells have a relatively high chloroplast density whose organellar membranes are composed mainly of unsaturated fatty acids (Hernández and Cejudo, 2021). Linoleate is an unsaturated fatty acid and is part of the chloroplast membrane. An increase in the degree of unsaturation of membrane lipids was associated with improved drought resistance and ROS neutralization (He and Ding, 2020a, Ullah et al., 2022, Zi et al., 2022), which highlights the potential role of fatty acid composition in poplar leaf palisade cells to help mitigate the L-WD stress-related consequences. Looking at leaf physiological parameters during WD stress (Supplementary Figure S1B),

409 compared to E-WD, photosynthesis, leaf conductance, and transpiration rates were improved during L-
410 WD, signifying the possible roles of flavonoids and fatty acids in neutralizing ROS (Jia et al., 2021, Resmi
411 et al., 2015), leading to the observed improved leaf performance during L-WD stress.

412 Vascular cells establish inter-tissue signaling via xylem and phloem sap, through which essential
413 metabolite classes, such as hormones, fatty acids, and sugars, are transported. Phloem cells were shown
414 to transport various fatty acids during normal and stress conditions (Guelette et al., 2012, Madey et al.,
415 2002). In our spatial MALDI-MS data, all three detected fatty acids (linoleate, hexadecanoic acid or
416 palmitic acid, and (6Z,9Z,12Z)-octadecatrienoic acid) were decreased in abundance in vascular cells during
417 E-WD stress conditions (Figure 3A, 3B, Supplementary Table S2). These results may indicate the
418 degradation of these fatty acids, via beta oxidation for energy production, as WD stress generally reduces
419 the photosynthetic carbon fixation capacity (Supplementary Figures S1). Activation of beta oxidation may
420 be associated to the increased levels of disaccharide and mono-saccharides and pentose phosphate
421 pathway-related metabolites during E-WD, possibly via gluconeogenesis pathway (Figure 3A, 3B).
422 Moreover, during recovery, our time-course MALDI-MSI analysis showed an opposite trend between fatty
423 acids and sugar abundance levels (Figure 3A, 3B), where we found an increased level of all three fatty
424 acids and decreased accumulation of sugars exclusively in vascular cells. This vascular cell-specific
425 opposite trend between fatty acid and sugar levels during WD stress and recovery conditions indicates
426 that vascular cells could possibly break down fatty acids to generate sugars during WD stress and re-
427 synthesize fatty acids during recovery (possibly by utilizing those sugars) as the demand for lipids is
428 increased during recovery from stress (Gigon et al., 2004). In addition, during recovery from stress, a lower
429 abundance was detected for many of the secondary metabolites exclusively in vascular cells
430 (Supplementary Table S2), highlighting the possibility that vascular cells diverted the carbon flow from
431 secondary metabolite biosynthesis to other essential pathways, such as fatty acid biosynthesis during WD
432 stress.

Water deficit stress imposes severe phenotypic damage to annual plants and perennial trees such as poplars. Annual plants escape from drought stress by allocating carbon to seed production, thereby advancing to the next generation. However, due to a longer reproductive cycles, perennial trees must withstand stress through different strategies such as tolerance or avoidance mechanisms involving stomatal regulation, synthesizing osmoprotectants, including ROS-neutralizing metabolites. Although more studies have been conducted on responses of annual plants to WD, there is a lack of understanding of metabolic responses of perennial trees to WD. In our work, we observed an overall reduction in poplar aboveground biomass during both early and late stress stages, while an increase in root biomass was observed in L-WD (compared to E-WD) (Supplementary Figure S1B). This could possibly be associated with the observed higher sugar levels in leaf-vascular cells during E-WD and their possible translocation to roots to reserve carbon for later usage or for root growth in response to WD stress. Carbon mobilization and storage in belowground sinks such as roots during dormancy followed by re-mobilization of carbon to support bud outgrowth in spring has been commonly reported in trees. On the other hand, in oak saplings (Heizmann et al., 2001), it was reported that under reduced photosynthetic condition, a higher-level carbon was translocated from roots to leaves via xylem sap. Our hypothesis on vascular cells-mediated sugar transport to support root growth or from root system to support shoot growth and development especially during WD should be further tested by isotope labeling and root metabolite profiling in future work. Stress memory is another emerging area where plants accumulate stress-responsive molecular signatures, enabling them to withstand future stress events (Tombesi et al., 2018). In our study, the recovery from WD was found to have higher levels of flavonoids in palisades and higher levels of fatty acids in vascular cells, possibly highlighting a preparedness for future episodes of WD stress.

We employed a GC-MS based approach to profile the whole leaf tissue metabolic changes under WD stress and recovery conditions, and then compared the outcome with the spatial distribution of metabolites derived by MALDI-MSI. However, we found only a few metabolites that showed similar

accumulation patterns between the spatial and whole tissue datasets (Figure 4A, 4B). This could be attributed to the inherent ionization, mechanical, and molecular selectiveness differences between these two mass spectrometry modalities. GC-MS is an efficient technique for detecting metabolites with mass weights typically < 500 Dalton, providing it with the ability to readily detect key compounds of primary metabolism including small organic acids and amino acids, and differentiate between sugar isomers (e.g., glucose, fructose, mannose, sorbose, etc.) (Smith and Morowitz, 2004). We detected 55 metabolites of these types with the GC-MS technique compared to the 16-20 metabolites detected by the MALDI-MSI technique. On the other hand, the MALDI-MSI capability used in this work is a powerful technique for detecting aromatic compounds and secondary metabolites. We detected about 73 metabolites of these types using MALDI-MSI compared to the 25 metabolites identified by the GC-MS approach (supplementary tables S2 and S3). Another possible explanation for the discrepancy between MALDI-MSI and GC-MS results is that since with MALDI-MSI we capture only a 10µm plane of the whole leaf, there is a chance that other areas of the leaf (within palisade and vascular regions) show a different trend of metabolite accumulations which in average could resemble the GC-MS output. However, this point is at least partially mitigated by a large number of biological and technical replicates used in this study for generating metabolic snapshots by MALDI-MSI. Moreover, a recent remarkable development in the MALDI-MSI approach, which uses a novel on-tissue chemical derivatization strategy (Zemaitis et al., 2023), has significantly expanded the metabolite coverage of phytocompounds including primary carbohydrates, amino acids, and TCA cycle compounds. This updated version of MALDI-MSI can be adopted in future studies to improve the cross-comparison between the whole tissue and spatial metabolomics techniques.

Overall, using spatial metabolomics, we found novel distinct WD-responsive metabolic maps of two major leaf cell types in poplar, which provide a better understanding on how different cell types work together to respond to environmental perturbations in a strategic perennial tree. Understanding spatiotemporal differences in metabolic responses to WD stress will help engineer targeted pathways in

specific cell types, potentially achieving maximum WD response and avoiding any pleiotropic effects on plant growth and yield.

Data availability statement

The datasets generated and analyzed during the current study will be made available in the respective data repositories shortly after submission. All the MALDI-MSI datasets and annotations will be publicly available at METASPACE. METASPACE links for reviewers:

- Positive ion mode analysis: https://metaspace2020.eu/api_auth/review?prj=e73ebe52-3b62-11ed-89bf-536c64910508&token=K3GB4ZCy0yDe
- Negative ion mode analysis: https://metaspace2020.eu/api_auth/review?prj=60c05570-3b80-11ed-89bf-0f161aeeebf3&token=sD4R5421iN8E

Author contributions

Vimal Kumar Balasubramanian designed and performed experiments, contributed to data analyses, wrote the original draft, reviewed, and edited the manuscript; **Dusan Velickovic** performed MALDI-MSI metabolomics and performed data analyses, reviewed, and edited the manuscript; **Maria Del Mar Rubio Wilhelmi** performed poplar water-deficit treatments and generated biomass data and helped generating GC-MS based whole tissue metabolomics data, reviewed, and edited the manuscript; **Christopher Anderton** assisted with the MALDI-MSI workflow development and data analysis, reviewed, and edited the manuscript; **Neal Stewart, Jr., Stephen DiFazio, and Eduardo Blumwald** acquired funding, reviewed, and edited the manuscript; **Amir H. Ahkami**: conceptualized the work, acquired funding, designed experiments, wrote and edited the manuscript.

Funding

This work was supported by funding from the Biological and Environmental Research (BER) in the U.S. Department of Energy (DOE) Office of Science, Genomic Science Program, Biosystems Design to Enable Next- Generation Biofuels (SyPro Poplar project, Award Number: DE-SC0018347). Part of this work was conducted at EMSL (Environmnetal Molecular Sciences Laboratory), a DOE Office of Science User Facility sponsored by the Office of Biological and Environmental Research and operated under Contract No. DE-AC05- 76RL01830, located at Pacific Northwest National Laboratory (PNNL).

Acknowledgments

We thank Dr. Albert Rivas Ubach (National Institute for Agricultural and Food Research and Technology (INIA-CSIC) for his help in one-way ANOVA analysis of the GC-MS metabolomics dataset.

Conflict of interest

The authors declare no conflicts of interest.

Figure Legends

Figure 1. Spatial metabolomics identified cell type-specific WD stress-responsive metabolites in Poplar leaf. (A). Total number of significantly altered metabolites under early water deficit (E-WD), late water deficit (L-WD), and recovery conditions identified through MALDI-MSI analysis. Metabolites significantly altered in two major leaf cell types, palisade (Pal.) and vascular (Vas.) cells, are marked with different bar patterns. The relative abundance level of each significant metabolite was averaged from 6 biological replicates with 2 technical replicates in any given condition. T-test was used for statistical analysis. Metabolites with significant (n=97, $p<0.05$) and moderate significant (n=7, $0.05<p\leq0.1$) changes are included. **(B).** Metabolites were grouped into various metabolic classes by Van Krevelen classification and

cell-type specificity of metabolites under each metabolic class were highlighted with green (Pal unique), brown (Vas unique) and grey (Pal and Vas shared metabolites) colors.

Figure 2. Palisade cell type-specific metabolites identified by MALDI-MSI analysis. **(A).** Metabolic pathway map of selected palisade cell-type abundant metabolites that were significantly altered during early (E), late (L) water-deficit stress and recovery (R) conditions. Metabolites with significant increased and decreased abundance levels during stress or recovery conditions compared to the control well-watered condition are presented by green and red colors, respectively. Metabolite relative abundance levels were averaged from 6 biological replicates with 2 technical replicates in any given condition. T-test was used for statistical analysis and metabolites that were significant ($p<0.05$) and moderately significant ($0.05<p \leq 0.1$) were used to generate heatmaps. Solid and dashed arrows represent direct and indirect metabolic pathway relationships, respectively. **(B).** Selective ion images of metabolites with palisade cell-type unique enrichment are shown. The ion image for each metabolite is a representative figure from 6 biological replicates with two technical replicates. Metabolite names with an asterisk (*) contain potential stereoisomers sharing the same molecular formula. For example, Quercetin* ($C_{15}H_{10}O_7$) and caffeate* ($C_9H_8O_4$) are shown as representative metabolites among the stereoisomers with same molecular formula. The scale bar is 1mm. WW: well-watered condition; WD: water-deficit stress.

Figure 3. Vascular cell type- specific metabolites identified by MALDI-MSI analysis. (A). Metabolic pathway map of selected vascular cell-type abundant metabolites that were significantly altered during early (E), late (L) water-deficit stress and recovery (R) conditions. Metabolites with significant increased and decreased abundance levels during stress or recovery conditions compared to the control well-watered condition are presented by green and red colors, respectively. Metabolite relative abundance levels were averaged from 6 biological replicates with 2 technical replicates in any given condition. T-test was used for statistical analysis and metabolites that were significant ($p<0.05$) and moderately significant ($0.05<p \leq 0.1$) were used to generate heatmaps. Solid and dashed arrows represent direct and indirect

552 metabolic pathway relationships, respectively. **(B)**. Selective ion images of metabolites with vascular cell-
553 type specific enrichment are shown. The ion image for each metabolite is a representative figure from 6
554 biological replicates with two technical replicates. Metabolite names with an asterisk (*) contain potential
555 stereoisomers sharing the same molecular formula. For example, sucrose* ($C_{12}H_{22}O_{11}$) and Glucose*
556 ($C_6H_{12}O_6$) are shown as representatives of disaccharides and monosaccharide stereoisomers, respectively.
557 The scale bar is 1mm. WW: well-watered condition; WD: water-deficit stress.

558 **Figure 4. Metabolite accumulations at whole leaf tissue level corresponds to spatially resolved**
559 **metabolites at cellular levels. (A).** Relative abundance levels of selective metabolites identified by whole
560 leaf tissue-based GC-MS metabolomics analysis under early water deficit (E-WD), late water deficit (L-
561 WD), and recovery conditions. Metabolite abundance is calculated from an average of 3 biological
562 replicates. One-way ANOVA was used for statistical analysis (** represents $p<0.05$). **(B).** Selective ion
563 images of monosaccharide, sugar phosphates, and fatty acids that show similar accumulation patterns
564 with whole leaf metabolite profiles during stress or recovery conditions are provided. For
565 monosaccharides and hexose phosphates, the ion abundance image reflects all stereoisomers with similar
566 molecular formula. Ion image for each metabolite is a representative figure from 6 biological replicate
567 with 2 technical replicates. T-test was used for statistical analysis ($0.1 \leq p<0.05$). Levels of metabolic shift
568 of each compound in stressed vs. control samples are shown by percentages in dark blue color. Pal:
569 palisade; Vas: vascular; ns: not significant; WW: well-watered condition; WD: water-deficit stress.

570

571 **Supplementary material**

572 **Supplementary Table S1:** Shoot and root biomass and gas exchange parameters (photosynthesis (A),
573 conductance (gs) and transpiration (E)) measured from early water deficit (E-WD) and late water deficit
574 (L-WD) stressed and recovered (R) poplar leaf tissue. Data averaged from four biological replicates for

biomass analysis and six biological replicates for leaf gas exchange parameters. t-test ($p<0.05$) was used for statistical analysis.

Supplementary Table S2: Total number of significantly altered metabolites identified through MALDI-MSI analysis of early water deficit (E-WD) and late water deficit (L-WD) stressed and recovered (R) poplar leaf tissue. Positive and negative ionization modes were used for data acquisition and non-overlapping metabolic features were merged. Metabolites were grouped into various metabolic classes by Van Krevelen classification, and cell-type unique (palisade unique and vascular unique) metabolites were separately tabulated from cell-type shared metabolites. Fold change values were calculated based on relative abundance of each metabolite in stress vs control conditions. T-test analysis was used for statistical analysis. Metabolites with significant ($n=97$, $p<0.05$) and moderate significant ($n=7$, $0.05<p<0.1$) changes are included.

Supplementary Table S3: Total number of significantly altered metabolites identified by whole leaf metabolite profiling using GCMS technique from early water deficit (E-WD) and late water deficit (L-WD) stressed and recovered (R) poplar leaf tissue. Fold change values were calculated based on relative abundance of each metabolite in stress vs control conditions. T-test analysis was used for statistical analysis ($p<0.05$).

Supplementary Table S4: Total number of significantly altered metabolites identified through negative ionization mode analysis in MALDI-MSI from early water deficit (E-WD) and late water deficit (L-WD) stressed and recovered (R) poplar leaf tissue. Fold change values were calculated based on relative abundance of each metabolite in stress vs control conditions. T-test analysis was used for statistical analysis and the data from this table is used to created Sup. Table S2.

Supplementary Table S5: Total number of significantly altered metabolites identified through positive mode analysis in MALDI-MSI from early water deficit (E-WD) and late water deficit (L-WD) stressed and recovered (R) poplar leaf tissue. Fold change values were calculated based on relative abundance of each

599 metabolite in stress vs control conditions. T-test analysis was used for statistical analysis and the data
600 from this table is used to created Sup. Table S2.
601
602 **Supplementary Figure S1. Water deficit stress alters plant dry weight and leaf physiological parameters**
603 **in poplar. (A.)** Shoot and root biomass and gas exchange parameters, photosynthesis (A), conductance
604 (gs) and transpiration (E) measured from plants exposed to early water deficit (E-WD) stress (30-35%
605 relative SWC), late water deficit (L-WD) stress (water level maintained for 10d at 30-35% relative SWC)
606 and recovery from stress (R) and data were collected. Data averaged from four biological replicates and
607 t-test was used for statistical analysis. *represents pvalue<0.05. (**B.)** Leaf samples were collected for whole
608 leaf tissue and spatial cell type specific metabolite profiling. Six biological replicates were harvested in any
609 given condition. Matrix-assisted laser desorption Ionization-mass spectrometry imaging (MALDI-MSI) and
610 Gas chromatography-mass spectrometry (GC-MS) analysis.
611 **Supplementary Figure S2. Cryosectioning of a poplar leaf tissue.** Cryosection highlighting mesophyll
612 palisade (p) and vascular (v) cell types used for MALDI MSI to generate spatial metabolome data. Scale
613 bar represents 300µm.
614 **Supplementary Figure S3. Whole leaf tissue-based metabolomics identified water deficit stress**
615 **responsive metabolites. (A.)** Total no. of metabolites significantly altered during early (E-WD) and late
616 (L-WD) water deficit stress and recovery (R) conditions in whole leaf tissue of poplar. Green and red bars
617 highlight metabolites with increased or reduced abundance levels during stress and recovery conditions.
618 Data averaged from three biological replicates and one-way ANOVA was used for statistical analysis
619 (p<0.05). (**B.)** Total significant metabolites were categorized into broader metabolic classes using KEGG
620 pathway analysis. The heatmap shows metabolite abundance levels in E-WD, L-WD and R conditions.
621 Data averaged from 3 biological replicates and ANOVA (p<0.05) was used for statistical analysis.
622

References

AHKAMI, A. H., WANG, W., WIETSMA, T. W., WINKLER, T., LANGE, I., JANSSON, C., LANGE, B. M. & MCDOWELL, N. G. 2019. Metabolic shifts associated with drought-induced senescence in Brachypodium. *Plant Science,* 289**,** 110278.

AHMED, U., RAO, M. J., QI, C., XIE, Q., NOUSHAHI, H. A., YASEEN, M., SHI, X. & ZHENG, B. 2021a. Expression Profiling of Flavonoid Biosynthesis Genes and Secondary Metabolites Accumulation in Populus under Drought Stress. *Molecules,* 26**,** 5546.

AHMED, U., RAO, M. J., QI, C., XIE, Q., NOUSHAHI, H. A., YASEEN, M., SHI, X. & ZHENG, B. 2021b. Expression Profiling of Flavonoid Biosynthesis Genes and Secondary Metabolites Accumulation in Populus under Drought Stress. *Molecules* [Online], 26.

ALBERT, N. W., THRIMAWITHANA, A. H., MCGHIE, T. K., CLAYTON, W. A., DEROLES, S. C., SCHWINN, K. E., BOWMAN, J. L., JORDAN, B. R. & DAVIES, K. M. 2018. Genetic analysis of the liverwort Marchantia polymorpha reveals that R2R3MYB activation of flavonoid production in response to abiotic stress is an ancient character in land plants. *New Phytologist,* 218**,** 554-566.

BARCHET, G. L., DAUWE, R., GUY, R. D., SCHROEDER, W. R., SOOLANAYAKANAHALLY, R. Y., CAMPBELL, M. M. & MANSFIELD, S. D. 2014. Investigating the drought-stress response of hybrid poplar genotypes by metabolite profiling. *Tree Physiol,* 34**,** 1203-19.

BARCHET, G. L. H., DAUWE, R., GUY, R. D., SCHROEDER, W. R., SOOLANAYAKANAHALLY, R. Y., CAMPBELL, M. M. & MANSFIELD, S. D. 2013. Investigating the drought-stress response of hybrid poplar genotypes by metabolite profiling. *Tree Physiology,* 34**,** 1203-1219.

BØGESKOV SCHMIDT, F., HESKES, A. M., THINAGARAN, D., LINDBERG MØLLER, B., JØRGENSEN, K. & BOUGHTON, B. A. 2018. Mass Spectrometry Based Imaging of Labile Glucosides in Plants. *Front Plant Sci,* 9**,** 892.

BRYANT, N. D., PU, Y., TSCHAPLINSKI, T. J., TUSKAN, G. A., MUCHERO, W., KALLURI, U. C., YOO, C. G. & RAGAUSKAS, A. J. 2020. Transgenic Poplar Designed for Biofuels. *Trends Plant Sci,* 25**,** 881-896.

COSSU, R. M., GIORDANI, T., CAVALLINI, A. & NATALI, L. 2014. High-throughput analysis of transcriptome variation during water deficit in a poplar hybrid: a general overview. *Tree Genetics & Genomes,* 10**,** 53-66.

CRUZ DE CARVALHO, M. H. 2008. Drought stress and reactive oxygen species: Production, scavenging and signaling. *Plant Signal Behav,* 3**,** 156-65.

DINNENY, J. R., LONG, T. A., WANG, J. Y., JUNG, J. W., MACE, D., POINTER, S., BARRON, C., BRADY, S. M., SCHIEFELBEIN, J. & BENFEY, P. N. 2008. Cell identity mediates the response of Arabidopsis roots to abiotic stress. *Science,* 320**,** 942-5.

DURAND, T. C., SERGEANT, K., RENAUT, J., PLANCHON, S., HOFFMANN, L., CARPIN, S., LABEL, P., MORABITO, D. & HAUSMAN, J. F. 2011. Poplar under drought: Comparison of leaf and cambial proteomic responses. *Journal of Proteomics,* 74**,** 1396-1410.

FÀBREGAS, N., LOZANO-ELENA, F., BLASCO-ESCÁMEZ, D., TOHGE, T., MARTÍNEZ-ANDÚJAR, C., ALBACETE, A., OSORIO, S., BUSTAMANTE, M., RIECHMANN, J. L., NOMURA, T., YOKOTA, T., CONESA, A., ALFOCEA, F. P., FERNIE, A. R. & CAÑO-DELGADO, A. I. 2018. Overexpression of the vascular brassinosteroid receptor BRL3 confers drought resistance without penalizing plant growth. *Nat Commun,* 9**,** 4680.

FARMER, A., THIBIVILLIERS, S., RYU, K. H., SCHIEFELBEIN, J. & LIBAULT, M. 2021. Single-nucleus RNA and ATAC sequencing reveals the impact of chromatin accessibility on gene expression in Arabidopsis roots at the single-cell level. *Mol Plant,* 14**,** 372-383.

FEISTEL, F., PAETZ, C., LORENZ, S. & SCHNEIDER, B. 2015. The Absolute Configuration of Salicortin, HCH-Salicortin and Tremulacin from Populus trichocarpa × deltoides Beaupré. *Molecules,* 20**,** 5566-5573.

GAO, Y., LIU, X., JIN, Y., WU, J., LI, S., LI, Y., CHEN, B., ZHANG, Y., WEI, L., LI, W., LI, R., LIN, C., REDDY, A. S. N., JAISWAL, P. & GU, L. 2022. Drought induces epitranscriptome and proteome changes in stem-differentiating xylem of Populus trichocarpa. *Plant Physiol,* 190**,** 459-479.

GIGON, A., MATOS, A. R., LAFFRAY, D., ZUILY-FODIL, Y. & PHAM-THI, A. T. 2004. Effect of drought stress on lipid metabolism in the leaves of Arabidopsis thaliana (ecotype Columbia). *Ann Bot,* 94**,** 345-51.

GORI, A., BRUNETTI, C., DOS SANTOS NASCIMENTO, L. B., MARINO, G., GUIDI, L., FERRINI, F., CENTRITTO, M., FINI, A. & TATTINI, M. 2021. Photoprotective Role of Photosynthetic and Non-Photosynthetic Pigments in Phillyrea latifolia: Is Their "Antioxidant" Function Prominent in Leaves Exposed to Severe Summer Drought? *International Journal of Molecular Sciences,* 22**,** 8303.

GUELETTE, B. S., BENNING, U. F. & HOFFMANN-BENNING, S. 2012. Identification of lipids and lipid-binding proteins in phloem exudates from Arabidopsis thaliana. *J Exp Bot,* 63**,** 3603-16.

HAMANISHI, E. T., BARCHET, G. L. H., DAUWE, R., MANSFIELD, S. D. & CAMPBELL, M. M. 2015. Poplar trees reconfigure the transcriptome and metabolome in response to drought in a genotype- and time-of-day-dependent manner. *BMC Genomics,* 16**,** 329.

HE, F., WU, Z., ZHAO, Z., CHEN, G., WANG, X., CUI, X., ZHU, T., CHEN, L., YANG, P., BI, L. & LIN, T. 2022. Drought stress drives sex-specific differences in plant resistance against herbivores between male and female poplars through changes in transcriptional and metabolic profiles. *Science of The Total Environment,* 845**,** 157171.

HE, M. & DING, N.-Z. 2020a. Plant Unsaturated Fatty Acids: Multiple Roles in Stress Response. *Frontiers in Plant Science,* 11.

HE, M. & DING, N. Z. 2020b. Plant Unsaturated Fatty Acids: Multiple Roles in Stress Response. *Front Plant Sci,* 11**,** 562785.

HEIZMANN, U., KREUZWIESER, J., SCHNITZLER, J.-P., BRÜGGEMANN, N. & RENNENBERG, H. 2001. Assimilate Transport in the Xylem Sap of Pedunculate Oak (Quercus robur) Saplings. *Plant Biology,* 3**,** 132-138.

HERNÁNDEZ, M. L. & CEJUDO, F. J. 2021. Chloroplast Lipids Metabolism and Function. A Redox Perspective. *Frontiers in Plant Science,* 12.

HODAEI, M., RAHIMMALEK, M., ARZANI, A. & TALEBI, M. 2018. The effect of water stress on phytochemical accumulation, bioactive compounds and expression of key genes involved in flavonoid biosynthesis in Chrysanthemum morifolium L. *Industrial Crops and Products,* 120**,** 295-304.

HONEKER, L. K., HILDEBRAND, G. A., FUDYMA, J. D., DABER, L. E., HOYT, D., FLOWERS, S. E., GIL-LOAIZA, J., KÜBERT, A., BAMBERGER, I., ANDERTON, C. R., CLIFF, J., LEICHTY, S., AMINITABRIZI, R., KREUZWIESER, J., SHI, L., BAI, X., VELICKOVIC, D., DIPPOLD, M. A., LADD, S. N., WERNER, C., MEREDITH, L. K. & TFAILY, M. M. 2022. Elucidating Drought-Tolerance Mechanisms in Plant Roots through 1H NMR Metabolomics in Parallel with MALDI-MS, and NanoSIMS Imaging Techniques. *Environmental Science & Technology,* 56**,** 2021-2032.

JEONG, J. S., KIM, Y. S., REDILLAS, M. C. F. R., JANG, G., JUNG, H., BANG, S. W., CHOI, Y. D., HA, S.-H., REUZEAU, C. & KIM, J.-K. 2013. OsNAC5 overexpression enlarges root diameter in rice plants leading to enhanced drought tolerance and increased grain yield in the field. *Plant Biotechnology Journal,* 11**,** 101-114.

JIA, H., WANG, L., LI, J., SUN, P., LU, M. & HU, J. 2020. Comparative metabolomics analysis reveals different metabolic responses to drought in tolerant and susceptible poplar species. *Physiologia Plantarum,* 168**,** 531-546.

716 JIA, J., ZHOU, J., SHI, W., CAO, X., LUO, J., POLLE, A. & LUO, Z.-B. 2017. Comparative transcriptomic
717 analysis reveals the roles of overlapping heat-/drought-responsive genes in poplars exposed to
718 high temperature and drought. *Scientific Reports,* 7**,** 43215.
719 JIA, X., GONG, X., JIA, X., LI, X., WANG, Y., WANG, P., HUO, L., SUN, X., CHE, R., LI, T., ZOU, Y. & MA, F.
720 2021. Overexpression of MdATG8i Enhances Drought Tolerance by Alleviating Oxidative Damage
721 and Promoting Water Uptake in Transgenic Apple. *Int J Mol Sci,* 22.
722 JIN, R., BAO, H., BAI, Y. & LI, X. 2011. Theoretical Study on the Antioxidant Activity of Alizarin, Purpurin,
723 and Pseudopurpurin. *In:* LIU, L. A., WEI, D. & LI, Y. (eds.) *Interdisciplinary Research and*
724 *Applications in Bioinformatics, Computational Biology, and Environmental Sciences.* Hershey, PA,
725 USA: IGI Global.
726 JORGE, T. F., MATA, A. T. & ANTÓNIO, C. 2016. Mass spectrometry as a quantitative tool in plant
727 metabolomics. *Philosophical Transactions of the Royal Society A: Mathematical, Physical and*
728 *Engineering Sciences,* 374**,** 20150370.
729 KUMAR, M., KUMAR PATEL, M., KUMAR, N., BAJPAI, A. B. & SIDDIQUE, K. H. M. 2021. Metabolomics and
730 Molecular Approaches Reveal Drought Stress Tolerance in Plants. *Int J Mol Sci,* 22.
731 LAW, S. R. 2020. Finding the metabolomic signature of drought resistance in poplar. *Physiologia*
732 *Plantarum,* 168**,** 529-530.
733 LEE, D. K., JUNG, H., JANG, G., JEONG, J. S., KIM, Y. S., HA, S. H., DO CHOI, Y. & KIM, J. K. 2016.
734 Overexpression of the OsERF71 Transcription Factor Alters Rice Root Structure and Drought
735 Resistance. *Plant Physiol,* 172**,** 575-88.
736 LEE, S. U., MUN, B. G., BAE, E. K., KIM, J. Y., KIM, H. H., SHAHID, M., CHOI, Y. I., HUSSAIN, A. & YUN, B. W.
737 2021. Drought Stress-Mediated Transcriptome Profile Reveals NCED as a Key Player Modulating
738 Drought Tolerance in Populus davidiana. *Front Plant Sci,* 12**,** 755539.
739 LI, X., YANG, Y., SUN, X., LIN, H., CHEN, J., REN, J., HU, X. & YANG, Y. 2014. Comparative Physiological and
740 Proteomic Analyses of Poplar (Populus yunnanensis) Plantlets Exposed to High Temperature and
741 Drought. *PLOS ONE,* 9**,** e107605.
742 LONG, T. A. 2011. Many needles in a haystack: cell-type specific abiotic stress responses. *Curr Opin Plant*
743 *Biol,* 14**,** 325-31.
744 MA, A. & QI, X. 2021. Mining plant metabolomes: Methods, applications, and perspectives. *Plant*
745 *Commun,* 2**,** 100238.
746 MADEY, E., NOWACK, L. M. & THOMPSON, J. E. 2002. Isolation and characterization of lipid in phloem
747 sap of canola. *Planta,* 214**,** 625-34.
748 NAKAYASU, E. S., NICORA, C. D., SIMS, A. C., BURNUM-JOHNSON, K. E., KIM, Y. M., KYLE, J. E., MATZKE,
749 M. M., SHUKLA, A. K., CHU, R. K., SCHEPMOES, A. A., JACOBS, J. M., BARIC, R. S., WEBB-
750 ROBERTSON, B. J., SMITH, R. D. & METZ, T. O. 2016. MPLEx: a Robust and Universal Protocol for
751 Single-Sample Integrative Proteomic, Metabolomic, and Lipidomic Analyses. *mSystems,* 1.
752 NOLAN, T. M., VUKAŠINOVIĆ, N., HSU, C. W., ZHANG, J., VANHOUTTE, I., SHAHAN, R., TAYLOR, I. W.,
753 GREENSTREET, L., HEITZ, M., AFANASSIEV, A., WANG, P., SZEKELY, P., BROSNAN, A., YIN, Y.,
754 SCHIEBINGER, G., OHLER, U., RUSSINOVA, E. & BENFEY, P. N. 2023. Brassinosteroid gene
755 regulatory networks at cellular resolution in the Arabidopsis root. *Science,* 379**,** eadf4721.
756 PLANT CELL ATLAS, C., JHA, S. G., BOROWSKY, A. T., COLE, B. J., FAHLGREN, N., FARMER, A., HUANG, S.-S.
757 C., KARIA, P., LIBAULT, M., PROVART, N. J., RICE, S. L., SAURA-SANCHEZ, M., AGARWAL, P.,
758 AHKAMI, A. H., ANDERTON, C. R., BRIGGS, S. P., BROPHY, J. A. N., DENOLF, P., DI COSTANZO, L.
759 F., EXPOSITO-ALONSO, M., GIACOMELLO, S., GOMEZ-CANO, F., KAUFMANN, K., KO, D. K.,
760 KUMAR, S., MALKOVSKIY, A. V., NAKAYAMA, N., OBATA, T., OTEGUI, M. S., PALFALVI, G.,
761 QUEZADA-RODRÍGUEZ, E. H., SINGH, R., UHRIG, R. G., WAESE, J., VAN WIJK, K., WRIGHT, R. C.,
762 EHRHARDT, D. W., BIRNBAUM, K. D. & RHEE, S. Y. 2021. Vision, challenges and opportunities for
763 a Plant Cell Atlas. *eLife,* 10**,** e66877.

PLOMION, C., LALANNE, C., CLAVEROL, S., MEDDOUR, H., KOHLER, A., BOGEAT-TRIBOULOT, M. B., BARRE, A., LE PROVOST, G., DUMAZET, H., JACOB, D., BASTIEN, C., DREYER, E., DE DARUVAR, A., GUEHL, J. M., SCHMITTER, J. M., MARTIN, F. & BONNEU, M. 2006. Mapping the proteome of poplar and application to the discovery of drought-stress responsive proteins. *Proteomics,* 6**,** 6509-27.

PRACHAROENWATTANA, I., CORNAH, J. E. & SMITH, S. M. 2005. Arabidopsis peroxisomal citrate synthase is required for fatty acid respiration and seed germination. *Plant Cell,* 17**,** 2037-48.

RESMI, M. S., VIVEK, P. J. & SONIYA, E. V. 2015. Over-expression of bael quinolone synthase in tobacco improves plant vigor under favorable conditions, drought, or salt stress. *FEBS Letters,* 589**,** 332-341.

RHEE, S. Y., BIRNBAUM, K. D. & EHRHARDT, D. W. 2019. Towards Building a Plant Cell Atlas. *Trends Plant Sci,* 24**,** 303-310.

ROBERTSON, S. M., SAKARIYAHU, S. K., BOLAJI, A., BELMONTE, M. F. & WILKINS, O. 2022. Growth-limiting drought stress induces time-of-day-dependent transcriptome and physiological responses in hybrid poplar. *AoB PLANTS,* 14.

ROSSO, L., CANTAMESSA, S., BERGANTE, S., BISELLI, C., FRICANO, A., CHIARABAGLIO, P. M., GENNARO, M., NERVO, G., SECCHI, F. & CARRA, A. 2023. Responses to Drought Stress in Poplar: What Do We Know and What Can We Learn? *Life (Basel),* 13.

RUBERT-NASON, K. F., HEDMAN, C. J., HOLESKI, L. M. & LINDROTH, R. L. 2014. Determination of salicinoids by micro-high-performance liquid chromatography and photodiode array detection. *Phytochem Anal,* 25**,** 185-91.

SARABIA, L. D., BOUGHTON, B. A., RUPASINGHE, T., VAN DE MEENE, A. M. L., CALLAHAN, D. L., HILL, C. B. & ROESSNER, U. 2018. High-mass-resolution MALDI mass spectrometry imaging reveals detailed spatial distribution of metabolites and lipids in roots of barley seedlings in response to salinity stress. *Metabolomics,* 14**,** 63.

SHEN, S., ZHAN, C., YANG, C., FERNIE, A. R. & LUO, J. 2023. Metabolomics-centered mining of plant metabolic diversity and function: Past decade and future perspectives. *Mol Plant,* 16**,** 43-63.

SHOMALI, A., DAS, S., ARIF, N., SARRAF, M., ZAHRA, N., YADAV, V., ALINIAEIFARD, S., CHAUHAN, D. K. & HASANUZZAMAN, M. 2022. Diverse Physiological Roles of Flavonoids in Plant Environmental Stress Responses and Tolerance. *Plants (Basel),* 11.

SINGH, P., ARIF, Y., BAJGUZ, A. & HAYAT, S. 2021. The role of quercetin in plants. *Plant Physiology and Biochemistry,* 166**,** 10-19.

SMITH, E. & MOROWITZ, H. J. 2004. Universality in intermediary metabolism. *Proceedings of the National Academy of Sciences,* 101**,** 13168-13173.

SOW, M. D., LE GAC, A.-L., FICHOT, R., LANCIANO, S., DELAUNAY, A., LE JAN, I., LESAGE-DESCAUSES, M.-C., CITERNE, S., CAIUS, J., BRUNAUD, V., SOUBIGOU-TACONNAT, L., COCHARD, H., SEGURA, V., CHAPARRO, C., GRUNAU, C., DAVIAUD, C., TOST, J., BRIGNOLAS, F., STRAUSS, S. H., MIROUZE, M. & MAURY, S. 2021. RNAi suppression of DNA methylation affects the drought stress response and genome integrity in transgenic poplar. *New Phytologist,* 232**,** 80-97.

TATTINI, M., GALARDI, C., PINELLI, P., MASSAI, R., REMORINI, D. & AGATI, G. 2004. Differential accumulation of flavonoids and hydroxycinnamates in leaves of Ligustrum vulgare under excess light and drought stress. *New Phytologist,* 163**,** 547-561.

TENORIO BERRÍO, R., VERSTAEN, K., VANDAMME, N., PEVERNAGIE, J., ACHON, I., VAN DUYSE, J., VAN ISTERDAEL, G., SAEYS, Y., DE VEYLDER, L., INZÉ, D. & DUBOIS, M. 2021. Single-cell transcriptomics sheds light on the identity and metabolism of developing leaf cells. *Plant Physiology,* 188**,** 898-918.

TOMBESI, S., FRIONI, T., PONI, S. & PALLIOTTI, A. 2018. Effect of water stress "memory" on plant behavior during subsequent drought stress. *Environmental and Experimental Botany,* 150**,** 106-114.

TSCHAPLINSKI, T. J., ABRAHAM, P. E., JAWDY, S. S., GUNTER, L. E., MARTIN, M. Z., ENGLE, N. L., YANG, X. & TUSKAN, G. A. 2019a. The nature of the progression of drought stress drives differential metabolomic responses in Populus deltoides. *Ann Bot,* 124**,** 617-626.

TSCHAPLINSKI, T. J., ABRAHAM, P. E., JAWDY, S. S., GUNTER, L. E., MARTIN, M. Z., ENGLE, N. L., YANG, X. & TUSKAN, G. A. 2019b. The nature of the progression of drought stress drives differential metabolomic responses in Populus deltoides. *Annals of Botany,* 124**,** 617-626.

ULLAH, S., KHAN, M. N., LODHI, S. S., AHMED, I., TAYYAB, M., MEHMOOD, T., DIN, I. U., KHAN, M., SOHAIL, Q. & AKRAM, M. 2022. Targeted metabolomics reveals fatty acid abundance adjustments as playing a crucial role in drought-stress response and post-drought recovery in wheat. *Frontiers in Genetics,* 13.

VELIČKOVIĆ, D., CHU, R. K., HENKEL, C., NYHUIS, A., TAO, N., KYLE, J. E., ADKINS, J. N., ANDERTON, C. R., PAURUS, V., BLOODSWORTH, K., BRAMER, L. M., CORNETT, D. S., CURTIS, W. R. & BURNUM-JOHNSON, K. E. 2021. Preserved and variable spatial-chemical changes of lipids across tomato leaves in response to central vein wounding reveals potential origin of linolenic acid in signal transduction cascade. *Plant Environ Interact,* 2**,** 28-35.

VELIČKOVIĆ, D., ROPARTZ, D., GUILLON, F., SAULNIER, L. & ROGNIAUX, H. 2014. New insights into the structural and spatial variability of cell-wall polysaccharides during wheat grain development, as revealed through MALDI mass spectrometry imaging. *Journal of Experimental Botany,* 65**,** 2079-2091.

WILKINS, O., WALDRON, L., NAHAL, H., PROVART, N. J. & CAMPBELL, M. M. 2009. Genotype and time of day shape the Populus drought response. *Plant J,* 60**,** 703-15.

WULLSCHLEGER, S. D., YIN, T. M., DIFAZIO, S. P., TSCHAPLINSKI, T. J., GUNTER, L. E., DAVIS, M. F. & TUSKAN, G. A. 2005. Phenotypic variation in growth and biomass distribution for two advanced-generation pedigrees of hybrid poplar. *Canadian Journal of Forest Research,* 35**,** 1779-1789.

XIAO, X., YANG, F., ZHANG, S., KORPELAINEN, H. & LI, C. 2009. Physiological and proteomic responses of two contrasting Populus cathayana populations to drought stress. *Physiologia Plantarum,* 136**,** 150-168.

XU, X. & JACKSON, D. 2023. Single-cell analysis opens a goldmine for plant functional studies. *Curr Opin Biotechnol,* 79**,** 102858.

YANG, B., MINNE, M., BRUNONI, F., PLAČKOVÁ, L., PETŘÍK, I., SUN, Y., NOLF, J., SMET, W., VERSTAEN, K., WENDRICH, J. R., EEKHOUT, T., HOYEROVÁ, K., VAN ISTERDAEL, G., HAUSTRAETE, J., BISHOPP, A., FARCOT, E., NOVÁK, O., SAEYS, Y. & DE RYBEL, B. 2021. Non-cell autonomous and spatiotemporal signalling from a tissue organizer orchestrates root vascular development. *Nature Plants,* 7**,** 1485-1494.

YANG, M., WANG, L., WANG, X., LI, Y. & HUANG, H. 2023. Transcriptomic Response to Drought Stress in Populus davidiana Dode. *Forests,* 14**,** 1465.

ZANG, Y., PEI, Y., CONG, X., RAN, F., LIU, L., WANG, C., WANG, D. & MIN, Y. 2023. Single-cell RNA-sequencing profiles reveal the developmental landscape of the Manihot esculenta Crantz leaves. *Plant Physiology*.

ZEMAITIS, K. J., LIN, V. S., AHKAMI, A. H., WINKLER, T. E., ANDERTON, C. R. & VELIČKOVIĆ, D. 2023. Expanded Coverage of Phytocompounds by Mass Spectrometry Imaging Using On-Tissue Chemical Derivatization by 4-APEBA. *Analytical Chemistry,* 95**,** 12701-12709.

ZHU, J., LOLLE, S., TANG, A., GUEL, B., KVITKO, B., COLE, B. & COAKER, G. 2023. Single-cell profiling of Arabidopsis leaves to Pseudomonas syringae infection. *Cell Rep,* 42**,** 112676.

857 ZI, X., ZHOU, S. & WU, B. 2022. Alpha-Linolenic Acid Mediates Diverse Drought Responses in Maize (Zea
858 mays L.) at Seedling and Flowering Stages. *Molecules,* 27.

859

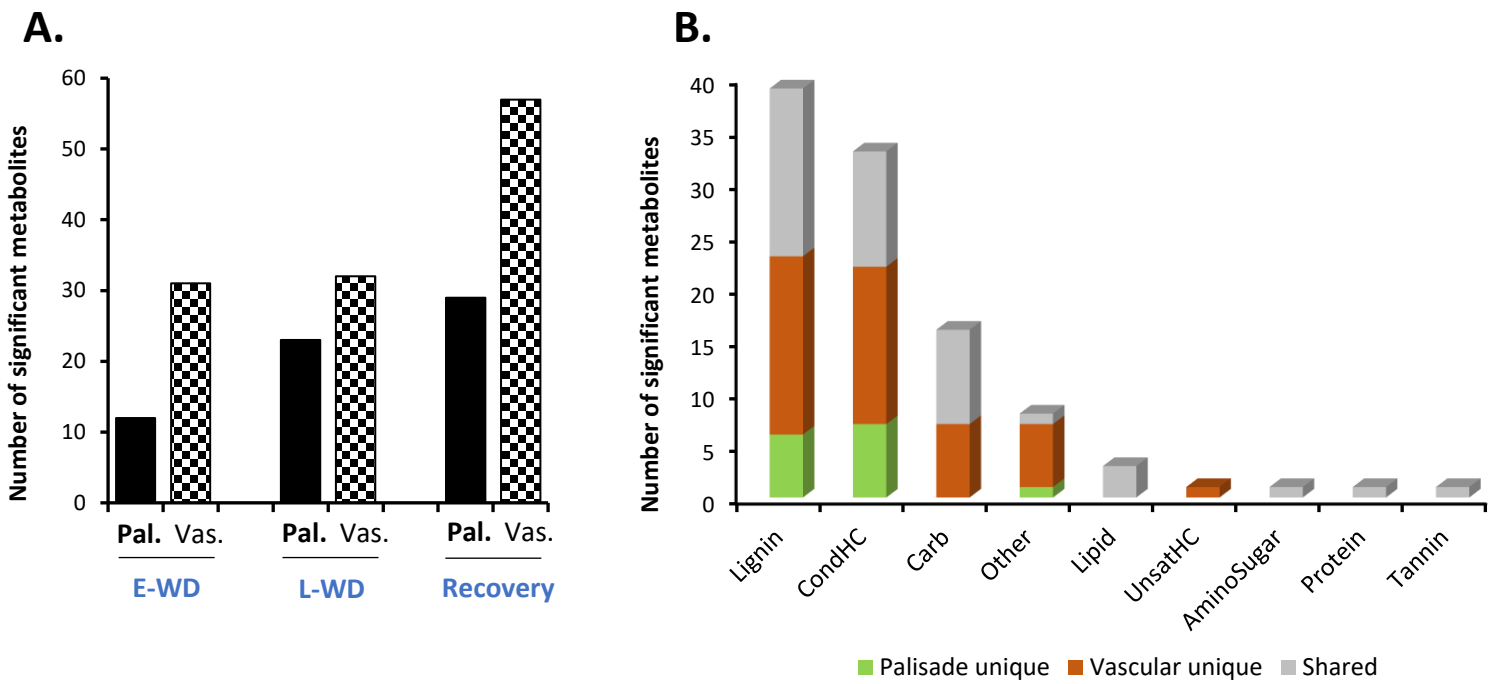

Figure 1. Spatial metabolomics identified cell type-specific WD stress-responsive metabolites in Poplar leaf. (A). Total number of significantly altered metabolites under early water deficit (E-WD), late water deficit (L-WD), and recovery conditions identified through MALDI-MSI analysis. Metabolites significantly altered in two major leaf cell types, palisade (Pal.) and vascular (Vas.) cells, are marked with different bar patterns. The relative abundance level of each significant metabolite was averaged from 6 biological replicates with 2 technical replicates in any given condition. T-test was used for statistical analysis. Metabolites with significant (n=97, $p<0.05$) and moderate significant (n=7, $0.05<p\leq0.1$) changes are included. **(B).** Metabolites were grouped into various metabolic classes by Van Krevelen classification and cell-type specificity of metabolites under each metabolic class were highlighted with green (Pal unique), brown (Vas unique) and grey (Pal and Vas shared metabolites) colors.

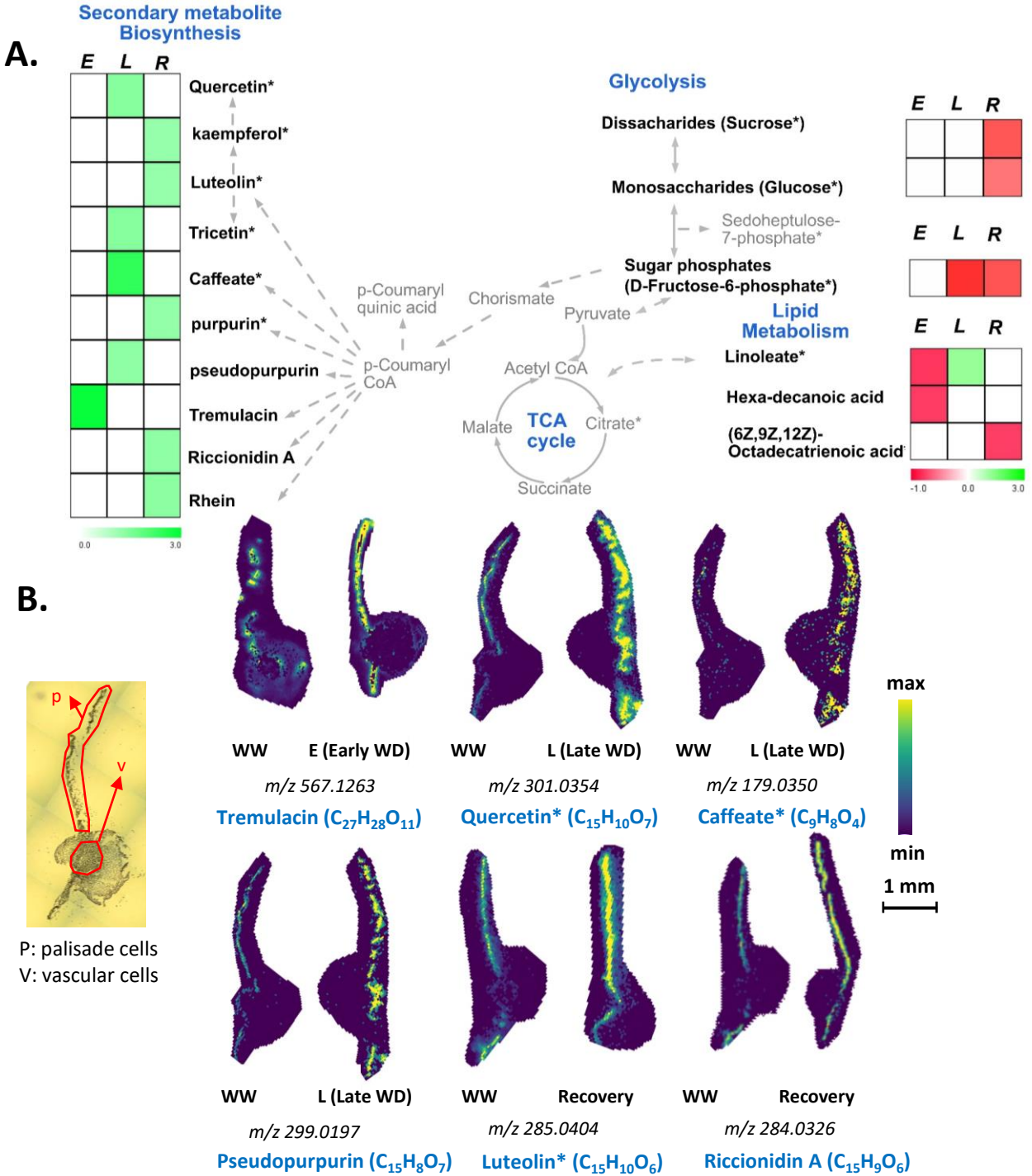

Figure 2. Palisade cell type-specific metabolites identified by MALDI-MSI analysis. (A) Metabolic pathway map of selected palisade cell-type abundant metabolites that were significantly altered during early (E), late (L) water-deficit stress and recovery (R) conditions. Metabolites with significant increased and decreased abundance levels during stress or recovery conditions compared to the control well-watered condition are presented by green and red colors, respectively. Metabolite relative abundance levels were averaged from 6 biological replicates with 2 technical replicates in any given condition. T-test was used for statistical analysis and metabolites that were significant ($p<0.05$) and moderately significant ($0.05<p \leq 0.1$) were used to generate heatmaps. Solid and dashed arrows represent direct and indirect metabolic pathway relationships, respectively. **(B)** Selective ion images of metabolites with palisade cell-type unique enrichment are shown. The ion image for each metabolite is a representative figure from 6 biological replicates with two technical replicates. Metabolite names with an asterisk (*) contain potential stereoisomers sharing the same molecular formula. For example, Quercetin* ($C_{15}H_{10}O_7$) and caffeate* ($C_9H_8O_4$) are shown as representative metabolites among the stereoisomers with same molecular formula. The scale bar is 1mm. WW: well-watered condition; WD: water-deficit stress.

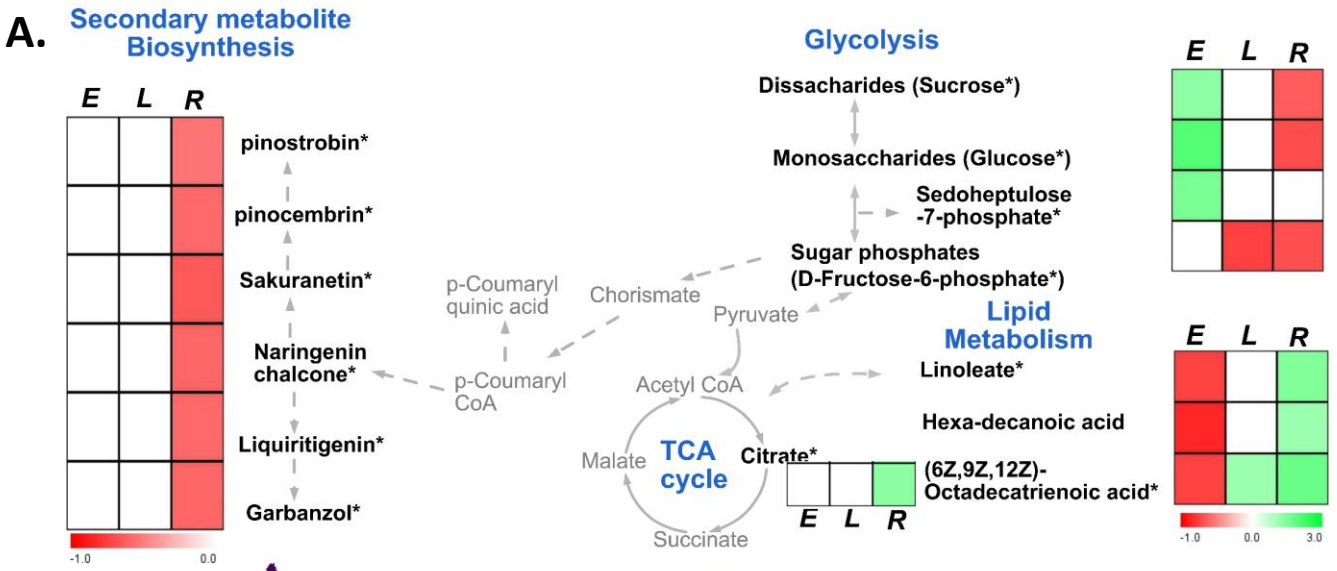

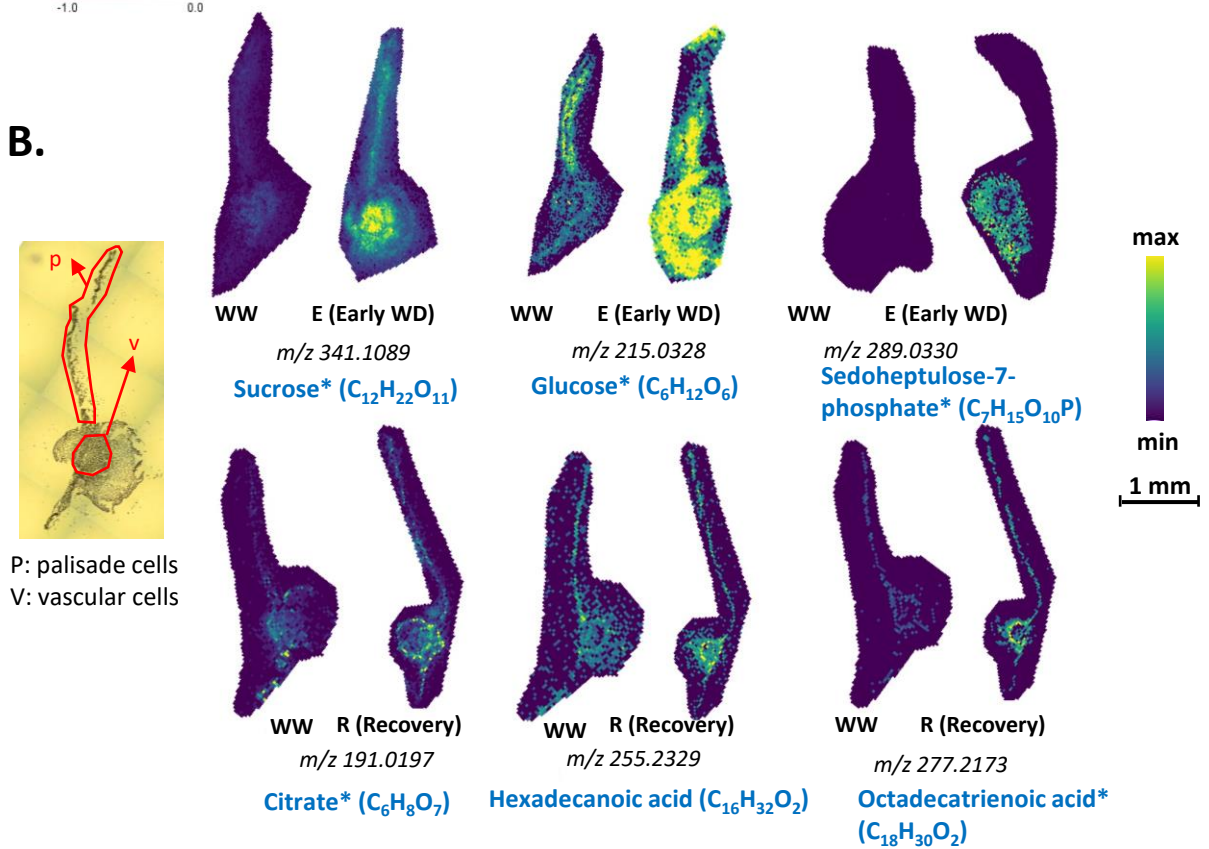

Figure 3. Vascular cell type- specific metabolites identified by MALDI-MSI analysis. (A) Metabolic pathway map of selected vascular cell-type abundant metabolites that were significantly altered during early (E), late (L) water-deficit stress and recovery (R) conditions. Metabolites with significant increased and decreased abundance levels during stress or recovery conditions compared to the control well-watered condition are presented by green and red colors, respectively. Metabolite relative abundance levels were averaged from 6 biological replicates with 2 technical replicates in any given condition. T-test was used for statistical analysis and metabolites that were significant ($p<0.05$) and moderately significant ($0.05<p \leq 0.1$) were used to generate heatmaps. Solid and dashed arrows represent direct and indirect metabolic pathway relationships, respectively. **(B)** Selective ion images of metabolites with vascular cell-type specific enrichment are shown. The ion image for each metabolite is a representative figure from 6 biological replicates with two technical replicates. Metabolite names with an asterisk (*) contain potential stereoisomers sharing the same molecular formula. For example, sucrose* ($C_{12}H_{22}O_{11}$) and Glucose* ($C_6H_{12}O_6$) are shown as representatives of disaccharides and monosaccharide stereoisomers, respectively. The scale bar is 1mm. WW: well-watered condition; WD: water-deficit stress.

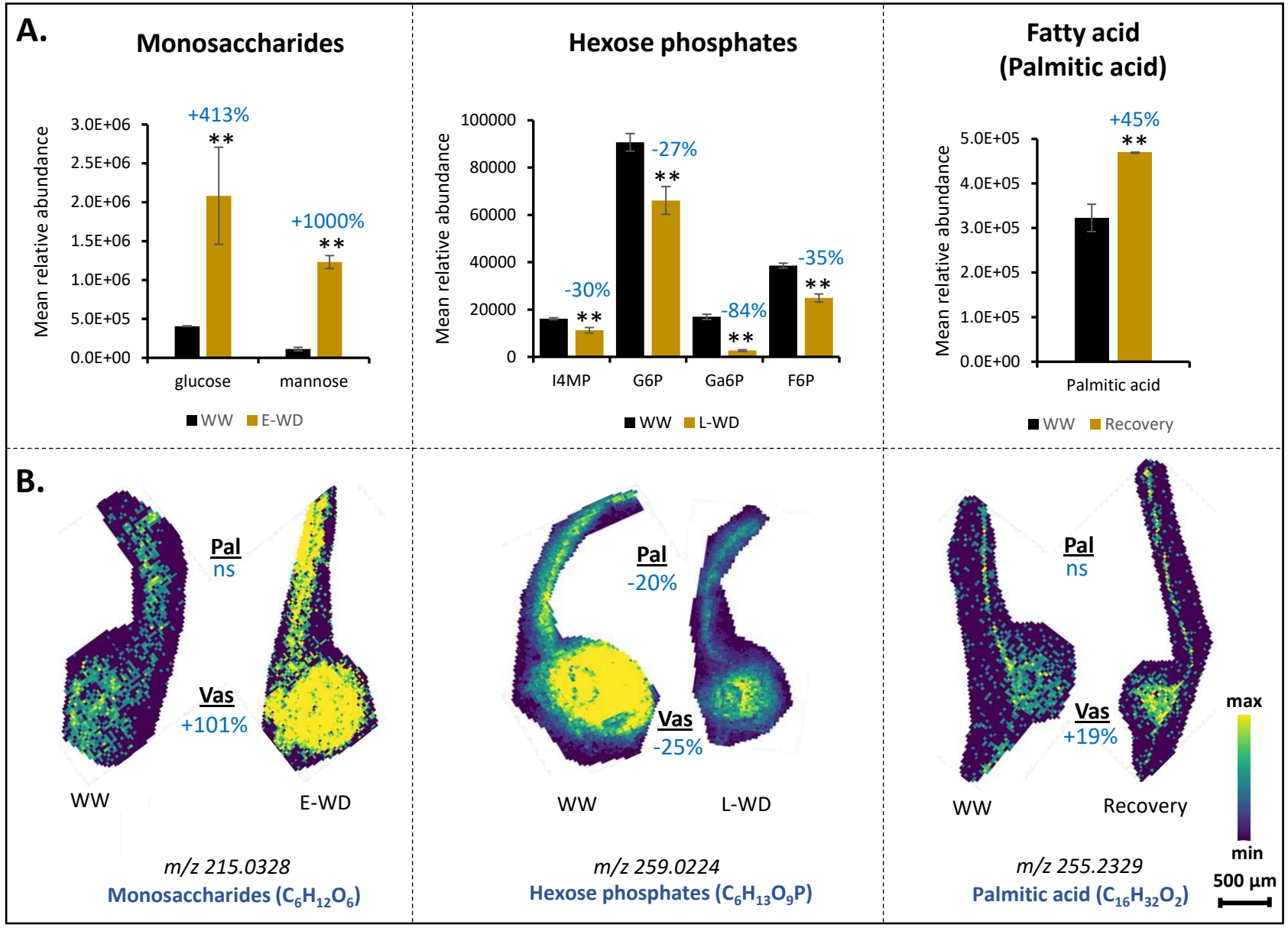

Figure 4. Metabolite accumulations at whole leaf tissue level corresponds to spatially resolved metabolites at cellular levels. (A) Relative abundance levels of selective metabolites identified by whole leaf tissue-based GC-MS metabolomics analysis under early water deficit (E-WD), late water deficit (L-WD), and recovery conditions. Metabolite abundance is calculated from an average of 3 biological replicates. One-way ANOVA was used for statistical analysis (** represents $p<0.05$). **(B)** Selective ion images of monosaccharide, sugar phosphates, and fatty acids that show similar accumulation patterns with whole leaf metabolite profiles during stress or recovery conditions are provided. For monosaccharides and hexose phosphates, the ion abundance image reflects all stereoisomers with similar molecular formula. Ion image for each metabolite is a representative figure from 6 biological replicate with 2 technical replicates. T-test was used for statistical analysis ($0.1 \leq p<0.05$). Levels of metabolic shift of each compound in stressed vs. control samples are shown by percentages in dark blue color. Pal: palisade; Vas: vascular; ns: not significant; WW: well-watered condition; WD: water-deficit stress.

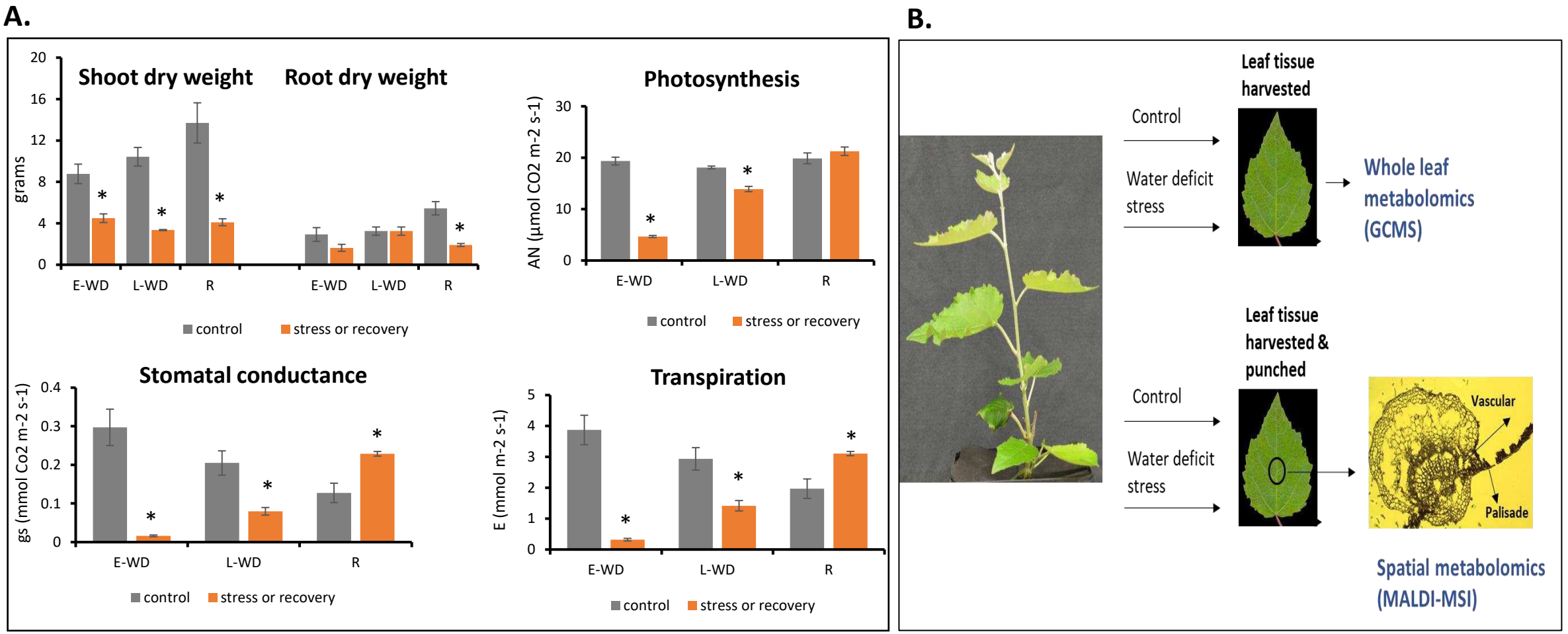

Supplementary Figure S1. Water deficit stress alters plant dry weight and leaf physiological parameters in poplar. A. Shoot and root biomass and gas exchange parameters, photosynthesis (A), conductance (gs) and transpiration (E) measured from plants exposed to early water deficit (E-WD) stress (30-35% relative SWC), late water deficit (L-WD) stress (water level maintained for 10d at 30-35% relative SWC) and recovery from stress (R) and data were collected. Data averaged from four biological replicates and t-test was used for statistical analysis. *represents pvalue<0.05. **B.** Leaf samples were collected for whole leaf tissue and spatial cell type specific metabolite profiling. Six biological replicates were harvested in any given condition. Matrix-assisted laser desorption Ionization-mass spectrometry imaging (MALDI-MSI) and Gas chromatography-mass spectrometry (GC-MS) analysis.

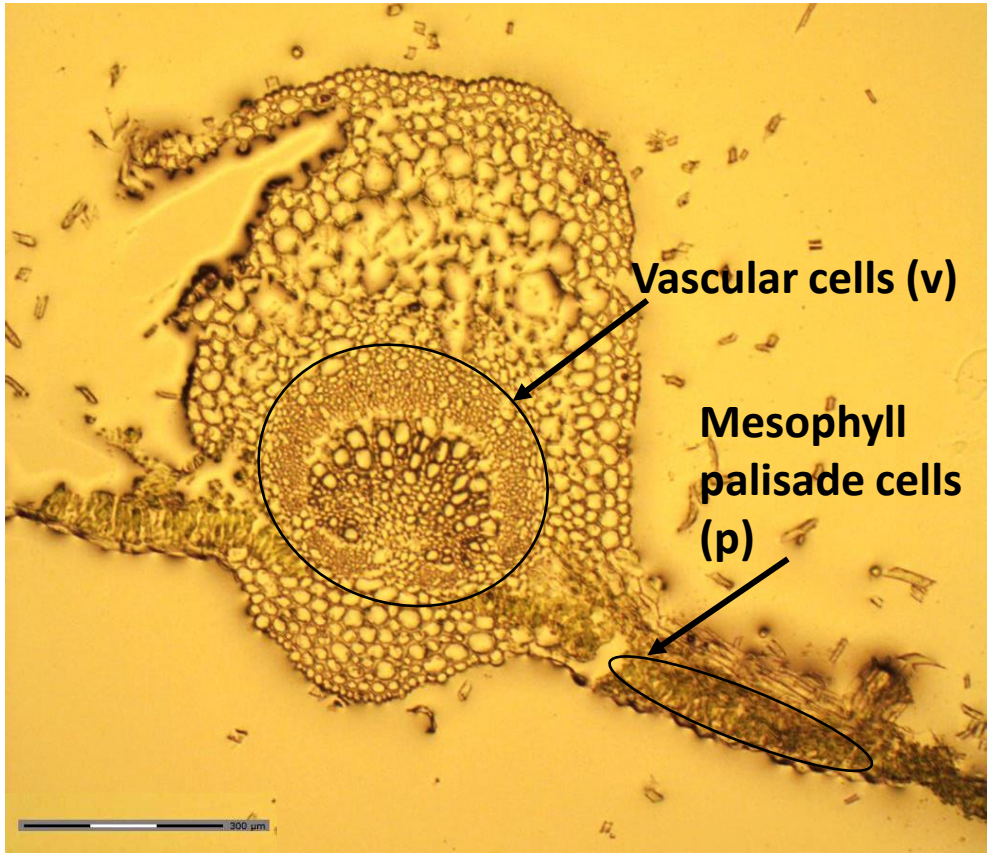

Supplementary Figure S2. **Cryosectioning of a poplar leaf tissue.** Cryosection highlighting mesophyll palisade (p) and vascular (v) cell types used for MALDI MSI to generate spatial metabolome data. Scale bar represents 300µm.

A.

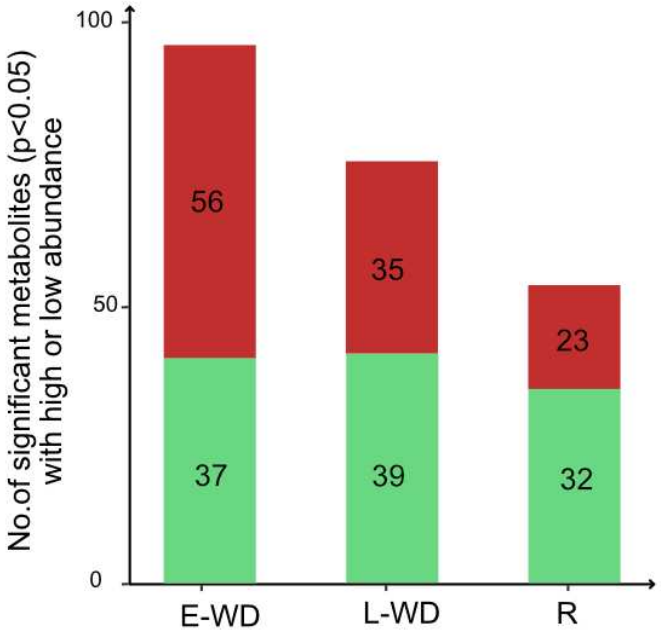

B.

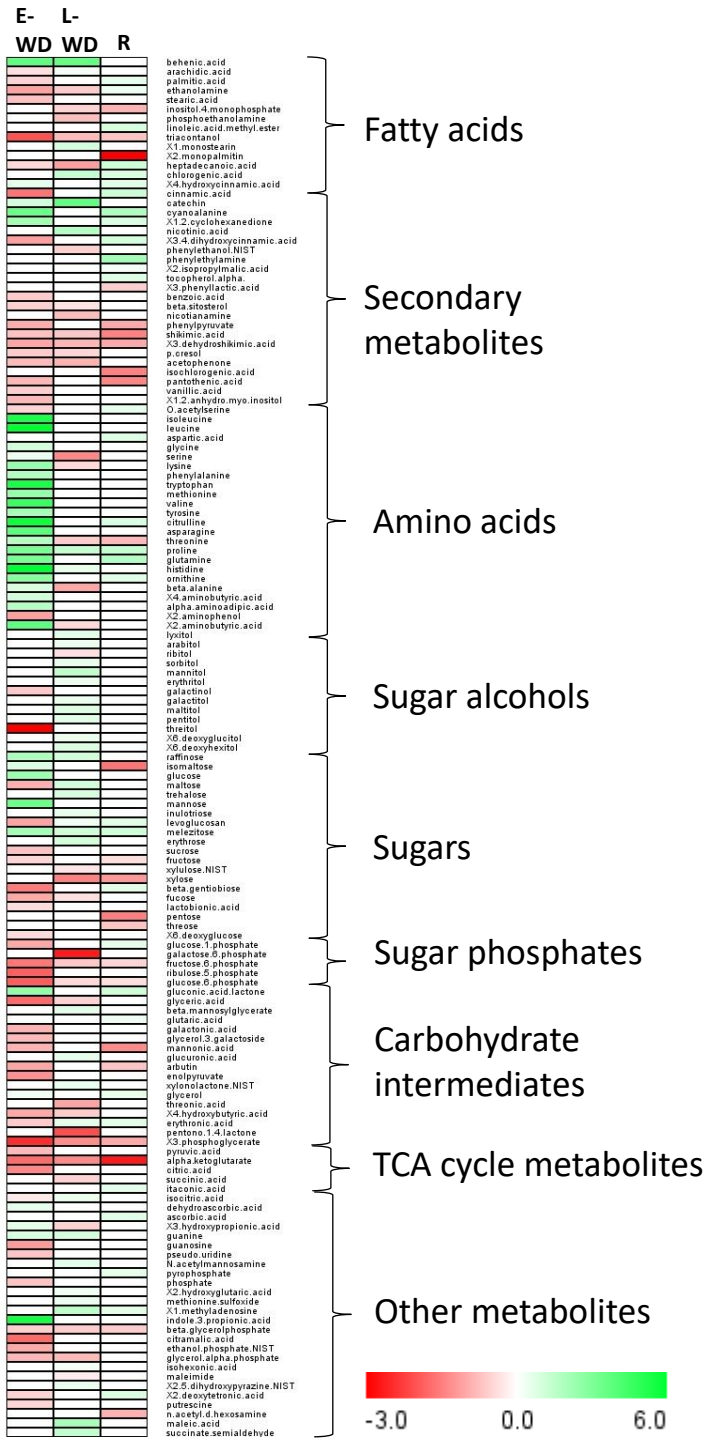

Supplementary Figure S3. Whole leaf tissue-based metabolomics identified water deficit stress responsive metabolites. A. Total no. of metabolites significantly altered during early (E-WD) and late (L-WD) water deficit stress and recovery (R) conditions in whole leaf tissue of poplar. Green and red bars highlight metabolites with increased or reduced abundance levels during stress and recovery conditions. Data averaged from three biological replicates and one-way ANOVA was used for statistical analysis ($p<0.05$). **B.** Total significant metabolites were categorized into broader metabolic classes using KEGG pathway analysis. The heatmap shows metabolite abundance levels in E-WD, L-WD and R conditions. Data averaged from 3 biological replicates and ANOVA ($p<0.05$) was used for statistical analysis.